HIGH FREQUENCY INTERNAL WAVES IN THE ST. LAWRENCE ESTUARY.

by

Jean-Claude Deguise

A thesis submitted to the Faculty of Graduate Studies and Research, McGill University, in partial fulfillment of the requirements for the degree of Master of Science.

Montreal August 1977

ABSTRACT

Topographically induced high-frequency (0.2-0.5 cycles/min) internal waves in a stratified medium are studied both from the theoretical point of view and from observations taken during the summer of 1975 in the middle estuary of the St. Lawrence River, near Pointe-au-Pic. Characteristics of the density and tidal current field in this part of the estuary during the summer (June-July) are presented. Different models (linear and non-linear) are used to explain the generation, properties and decay of the observed high-frequency internal waves. The importance of vertical shear of the horizontal velocity is also discussed. A description of the internal waves is given, accompanied by the current and density values prevailing at the time of the observations. The waves are observed over short intervals of time, usually 10 to 20 minutes, when the Richardson number takes its lowest values. The waves rapidly became non-linear and exhibited characteristics similar to those of solitary waves. "Blocking" effects upstream of the obstacle are also evident.

RESUME

Le phénomène des ondes internes de haute fréquence (0.2-0.5 cpm) créées derrière un obstacle dans un fluide stratifié est étudié autant du point de vue théorique qu'à partir d'observations prises durant l'été de 1975 dans l'estuaire moyen du St-Laurent près de Pointe-au-Pic. Des valeurs de courant et de densité caractéristiques de cette région durant l'été (Juin-Juillet) sont présentées. Une valeur moyenne du gradient vertical de la vitesse est également évalué. Différents modèles (linéaires et non-linéaires) sont utilisés pour expliquer la génération, les propriétés et la dégradation des ondes internes de haute fréquence observées près de Pointe-au-Pic. Enfin une description de ces ondes internes est accompagnée des données de courant et de densité qui prévalaient au moment des observations. Leur durée est d'environ 10 à 20 minutes alors que le nombre de Richardson est à son plus faible. Ces ondes internes deviennent rapidement non-linéaires et peuvent être classées dans la catégorie des ondes solitaires. Des effets de "blocage" à l'avant de l'obstacle sont également évidents.

ACKNOWLEDGEMENTS

The author wishes to thank all those people who helped in the completion of this thesis, in particular the Groupe Interuniversitaire de Recherches Océanographiques du Québec for financial and logistic support, the crew of the M/V METRIDIA, and Miss Patricia Chwartkowski for the correction of the first manuscript. I would also like to thank my thesis director, Professor R.G. Ingram, for his helpful suggestions and constant encouragement during my studies.

TABLE OF CONTENTS

LIST OF FIGURES

Page

LIST OF TABLES

CHAPTER 1

INTRODUCTION

1.1 INTRODUCTION

This thesis will be devoted to the study of a natural phenomenon called internal waves. Even though their existence is well known, internal waves are not very well understood, because of the difficulty in describing their characteristics. The best known external manifestations of internal waves in fluids are the cloud patterns often found behind mountain ranges, the "dead-water" phenomenon in certain highly stratified waters, surface slicks occurring on the sea surface, and observations in certain laboratory experiments (e.g., Long, 1955).

The importance of internal waves and their role in nature is not very well known. We do know that they have in certain cases a large influence on surface currents (e.g., Forrester, 1974), that they increase mixing of different water masses and that they may cause significant changes in the local distribution of nutrients and other water properties in shallow areas. Therefore, it is certain that internal waves, similar to those reported in this work, do significantly perturb in one way or another the marine environment and the life within it.

Numerous studies have already been devoted to describing internal waves of long period (hours), usually of tidal origin, but fewer people have looked at shorter period (a few minutes) phenomena. It is a difficult problem to distinguish high-frequency internal waves from the natural turbulence present in the sea within the same range of frequency. Furthermore, to understand the behaviour of these waves, wavelength, frequency, shape, amplitude, and many other properties of the ambient fluid have to be measured simultaneously at more than one location. For example, the vector velocity of the current, the vertical shear of the horizontal velocity field and the density stratification must be obtained in order to compare observations and existing theory on internal waves.

In the ocean many factors can cause the generation of internal waves (see Thorpe, 1975). They can be created by the tide, atmospheric pressure disturbances and current shear in the presence of a stratified water column. In the present work, we were specifically interested in those that occur behind an obstacle in the flow, classically called "lee-waves". These waves were first studied by meteorologists behind mountain ranges, and later were noticed in the ocean and in many estuaries and bays of the world.

This thesis is based on observations taken in the St.Lawrence estuary and will treat the generation of high-frequency internal waves behind a submerged obstacle (a bank in the middle of the river). The regular appearance of these waves (occurring almost every cycle of the semi-diurnal tide), their small horizontal scale and their proximity to an area of rapidly changing biological and sedimentological properties provided a great stimulus in the pursuit of this study.

In this thesis, I shall describe a series of high frequency oscillations of the density field in an estuarine environment. Most of the events described are believed to be internal waves, generated by bottom topographic irregularities. A general description of tidal circulation and isopycnal distribution is also given, so as to describe conditions during the internal wave observations. Prior to a discussion of the field data, a summary of the relevant theoretical considerations is presented in Chapter 2.

1.2 DEFINITIONS AND METHODS

The reader should note that all directions mentioned in this paper are relative to True North (T.N.) and positive in the clockwise direction. The time used is Eastern Standard Time (E.S.T.). All averages of vector properties will be assumed to be a vector average unless otherwise stated. Current meter observations were made with an Aanderaa RCM (sampling interval = 30 sec), while salinity-temperature profiles were done with an Inter-Ocean 513A.

CHAPTER 2

INTERNAL WAVES

2.1 INTRODUCTION

> "We have very little knowledge of which physical processes are most important in controlling internal gravity waves in the deep ocean. We do not know precisely how or even where internal waves are generated. We do not know how, by the propagation and interaction of waves, the observed spectral shapes are established. We do not know what processes dominate in the dissipation of internal waves."
>
> Thorpe (1975)

Thorpe's citation refers to deep ocean waves but is just as appropriate for estuaries where a wide variability in space and time often makes the problem more complex. For many years now, researchers in meteorology, oceanography and engineering have been interested in the subject of internal waves. A large number of sophisticated theories have been put forth in an effort to understand the phenomenon, leaving us with a hard choice, especially when one tries to apply theory to field observations made at a particular location. Most models do not include appropriate conditions or are incomplete.

One approach is to describe the subject in three logical steps: generation, propagation and decay. The authors cited below have usually treated these topics separately. The different aspects of the theory should, however, respect the same basic hypothesis and be complementary to one another as much as possible.

2.2 GENERATION

Many ideas have been put forward and proved useful in explaining why and how coherent oscillations can be generated in a stratified fluid. Past experience shows us that internal waves exist in so many different situations that any scientist interested in this study has to start with a preconceived idea (a starting hypothesis) of what he is looking for and where he is to find it. In this case, the possibility of internal waves in the study region was suggested from data taken for another purpose. After examining a bathymetric chart of the region (and having no information on the current and density values), the most plausible reason for the oscillations is the bottom topography (lee waves). Right or wrong, this intuitive choice will orient one's data collection as well as one's interpretation of these data.

This choice was further reinforced by the circulation pattern, which will be described in Chapter 3. Water flows on each side of the English Bank, creating in the narrow north-west passage adjacent to the mainland the appropriate conditions for the appearance of lee waves: (i) large obstacle (70% of the total depth of the channel),

(ii) moderate density stratification, and (iii) suitable shear conditions in some instances.

Internal waves have been studied for many years, but it was R.R. Long of John Hopkins University[1] who was one of the first to have extensively treated the subject of high-frequency lee waves. Although this work was published over twenty years ago, its explanation remains simple and close enough to the physical situation to be of interest in our case. Furthermore, the current and density distribution in the area of our study closely approximate those required in Long's theories.

As long as the obstacle is neither sharp nor abrupt, its shape is of little importance to the theory. Knowing the height of the barrier (relative to the surrounding flat horizontal bottom), Long determined for what conditions of current and density stratification oscillations will exist. His theoretical developments were supported by a remarkable series of laboratory experiments that gave much credibility to his mathematical treatment.

He was concerned with the two-dimensional steady state motion of an incompressible, inviscid, stratified fluid in a horizontally

---

[1] See Long, 1953, 1955.

infinite channel $(-\infty < x < \infty)$ with rigid and parallel upper and lower boundaries.

The two dimensionality of the flow required the neglect of the Coriolis effect, which is also applicable here because of the small scale of the waves (assumed to be order of one km or less) and because of the short period of these waves (2-3 minutes) compared with the inertial period. The steady state requirement, on the other hand, is not appropriate for conditions in the St. Lawrence estuary. However, the fact that high-frequency internal waves have been observed for time intervals of only 20 to 60 minutes allows one to consider the background tidal flow as a quasi-static medium.

Another difference between Long's model and the real physical situation is his assumption of an inviscid fluid in a bounded channel. As McIntyre (1972) suggests, an unbounded viscous medium (like the estuary) can only support decaying wave phenomena. As Long's theory is used to examine only the generation of the waves, it does not matter if it deals with decaying or permanent waves (no viscosity). The viscous effects will only change the shape and the reabsorption of the waves.

In an early publication, Long (1953) derived the equation of motion for the stratified flow as described above, in which velocity and density are only a function of z (vertical axis) and are defined far upstream (negative x-direction) where he assumed the flow to be undisturbed. He also defined a streamfunction Ψ which varies monotonically with z, such that the longitudinal velocity $u = \partial\Psi/\partial z$, the vertical velocity $-w = \partial\Psi/\partial x$ and the density ρ are unique functions of ψ (i.e. streamlines represent isopycnals). Note that because of the monotonicity of the streamfunction there should be no reversal of the flow in any vertical section.

The full inviscid equations and the preceeding assumptions lead to the following equation for the streamfunction ψ (Long, 1953):

$$\nabla^2\psi + \frac{1}{\rho}\frac{d\rho}{d\psi}\left[\frac{1}{2}(u^2 + w^2) + gz\right] = f(\psi) \qquad (2.1)$$

where f (ψ) is a specified function of ψ. This equation is highly non-linear except if one chooses a particular initial density and velocity distribution.

If both the density gradient, $d\rho/dz$, and the dynamic pressure, $\frac{1}{2}\rho U^2$, are assumed constant upstream of the barrier, equation (2.1) is simplified greatly. With η being the displacement of streamlines from their initial level (Z_0), Long reduces equation (2.1) to

$$\nabla^2\eta + J\,\eta = 0 \qquad (2.2)$$

where $\eta = Z - Z_0$ and $J = \dfrac{g\left|\dfrac{1}{\rho}\dfrac{d\rho}{dz_o}\right|}{U^2} = \dfrac{N^2D^2}{U^2}$, also called the overall Richardson number (see Turner (1973) for a definition). N is the Brunt-Väisälä frequency based on the linear density distribution away from the source (or before the beginning of the perturbation) and U is the constant speed of the flow (no shear) at the same location. This particular kind of flow corresponds quite well to what was observed in the region of our study (see Chapter 3). It should also be noted that the space variables are dimensionless, having been scaled to the total depth of the channel D; J should then be considered as a pure number.

As it is almost impossible to find a solution to the above equation when the flow is over a finite obstacle, many researchers use an indirect method. As a first step, Long used Fourier integrals to obtain the streamlines for a rounded infinitesimal barrier (at x = 0). The resulting curve $Z_0 = 0$ corresponds everywhere to the bottom of the channel except near the origin where it rises and deviates from the exact shape of the obstacle. The amount of deviation is controlled by the shape of the obstacle and can be increased to finite values. The final step is to replace this small obstacle by another one which has the same shape as the above bottom streamline; with the new obstacle the flow automatically satisfies the boundary conditions. The disadvantage of this method is that the shape of the barrier cannot be predicted a priori and only particular obstacle shapes, sometimes asymmetric about the line x = 0, can be found to satisfy the boundary equations.

Long's main conclusion was that for a particular barrier of finite height, the existence of a solution depends on J or the flow conditions. He developed a relation between the relative height of the obstacle (compared with the channel) and J; if one knows the barrier height, a range of values for J can be calculated for which lee-waves can exist. With the same conditions, Huppert and Miles (1969) arrived at a similar conclusion for an infinite half-plane space.

Another point to consider in Long's early theories is the question of "upstream influence". Aware of the problem, Long simply neglected the possibility of "columnar disturbances" which could change upstream conditions. The subject of upstream disturbances was treated in a later paper (Long, 1970).

Unfortunately the depth (D) of our channel is not constant, making it difficult to determine the relative amplitude of the sill compared to the total depth of the channel. The obstacle is certainly large, representing over half the channel depth, when compared to the deepest part of the downstream section (over 180 m). With such a large obstacle non-linear effects can be expected to appear, thus making Long's linear model non-applicable. Even so, the preceding discussion of Long's model provides some insight into some possible mechanisms. It is also useful in determining what flow conditions are suited for the appearance of lee-waves. For such a large obstacle, Long predicts the existence of waves only when $J < \pi$.

More recently, Bell (1975) studied the generation of internal gravity waves by the simple harmonic flow of a stably stratified fluid over an obstacle. He examined the general problem with no upper boundary. Assuming that the obstacle was a small localized disturbance, he found that the energy propagated away from the source region in the form of an internal gravity wave field. The angle of propagation of the wave front in the vertical was dependent on the stratification. Furthermore, the solution suggested that different harmonics are sensitive to varying features of the obstacle: the waves of fundamental frequency being sensitive to the slope of the obstacle, the first harmonic to its curvature and so forth for the higher harmonics. Although interesting, the theory is not directly applicable to the present study, as the sill near Pointe-au-Pic is very large compared to the total depth of the water and cannot be considered as a small localized disturbance.

Gargett (1976) proposed a different mechanism to explain the generation of internal waves in the Strait of Georgia (British Columbia). The wave characteristics that she describes are similar to those which will be discussed in the present work. In-situ observations, combined with aerial photography, permitted her to describe the wave properties. The field results suggested that a submarine ridge acted as a boundary between a well-mixed and a stratified water mass at an inter-island pass. The generation mechanism was in the form of an impulsive disturbance through the pass to the stratified water mass of the Strait. This occurred at times of abruptly changing tidal flows. Linear and non-linear effects were discussed.

Halpern (1971) observed short-period internal waves in Massachusetts Bay very similar to the type of waves described in this thesis. Although he did not clearly understand the mechanism of wave generation, Halpern suggested that the abrupt rise in temperature accompanying a discrete group of short-period internal waves and the subsequent formation of these groups are probably due to shearing instability in the tidal flow when the current floods over the crest of an upstream bank. In contrast, theoretical arguments by Lee and Beardsley (1974) suggest that neither shear instability nor a quasi-steady lee wave mechanism was responsible for wave generation. They assume that the temperature rise results from "blocking" by the bank and non-linear properties associated with the front. As a result of dispersion and non-linear effects, large amplitude internal waves are generated at the front.

2.3 WAVE PROPERTIES

In considering the properties and propagation of internal waves, the classical linear theory will be presented first, to be followed by a discussion of non-linear effects.

In the region of a diffuse pycnocline and weak mean shear, the Brunt-Väisälä frequency and the vertical velocity gradient can, locally, be considered constant. For these conditions, Phillips (1966), using the method of asymptotic expansions described by Erdelyi (1956), found a solution for the governing equations of motion. He obtained an equation for the vertical component of the velocity:

$$W \simeq G(1+\beta^2 t^2 \cos^2\phi)^{-3/4} \exp\left\{i\,(kx+ly-\beta t k z)\right\} \exp\left\{\,i\Omega(t)\right\} \tag{2.4}$$

where $\beta = \partial U/\partial z$ is the mean rate of shear; $\cos\phi = k/(k^2+l^2)^{\frac{1}{2}}$ specifies the initial orientation of the wave number vector (k, l) in the horizontal plane; G is an arbitrary constant and

$$\Omega(t) = \frac{N}{\beta\cos\phi}\int^{\beta t\cos\phi}(1+T^2)^{-\frac{1}{2}}\,dT\,, \tag{2.5}$$

where $T = \beta t\cos\phi$.

The vertical displacement of a fluid element is

$$\zeta = -i\frac{G}{N}(1+\beta^2 t^2\cos^2\phi)^{-\frac{1}{4}}\exp\left\{i(kx+ly-\beta tkz)\right\}\exp\left\{i\Omega(t)\right\} \qquad (2.6)$$

The wavelength continually diminishes as the wave-number magnitude $(k^2+l^2+\beta^2t^2k^2)^{\frac{1}{2}}$ increases with time. An important effect of the shear is to rotate the direction of the wave-number vector in the vertical plane. The expression for the angle θ of the wave-number vector and the horizontal is

$$\cos\theta = \left\{\frac{k^2+l^2}{k^2+l^2+\beta^2t^2k^2}\right\}^{\frac{1}{2}} = (1+\beta^2t^2\cos^2\phi)^{-\frac{1}{2}}. \qquad (2.7)$$

One notes that when $\beta t\to\infty$, the wave-number vector becomes vertical ($\theta\to\pi/2$) and the motion tends towards the steady horizontal sliding of each layer past the next.

The frequency of the wave is

$$\omega = \frac{d\Omega(t)}{dt} = N(1+\beta^2t^2\cos^2\phi)^{-\frac{1}{2}} = N\cos\theta$$ and is largest for $\theta = 0^0$, when $\omega = N$. Another consequence of this limitation is that the

waves are confined to a layer where N is larger than the wave frequency. Note finally that ω is independent of the wave-number magnitude and is only a function of its direction.

The phase velocity of the waves is $C = \omega / K$ with K being the wave-number amplitude and the group velocity being $C_g = \frac{C}{\cos\theta} - C = \frac{N - \omega}{K}$.

Note that $C_g \rightarrow 0$ when $\omega \rightarrow N$.

As previously mentioned in section 2.1, non-linear effects can be very important if the obstacle in the channel is large compared to the total depth of the fluid. Gargett (1976) explained the properties of her waves by using a non-linear approach. She used a two layer model in which the thin top-layer is of slowly varying density and the deep bottom layer is of constant density. The classical linear theory was sufficiently accurate to describe the shape of the waves but failed to predict the wavelength and the spacing between each group. Considering first order non-linear effects in the wave equation (of the initial value problem), she obtained a straightforward solution for the constant density bottom layer. For the thin upper layer with varying density, the solution was more complex. Using the boundary conditions at the bottom and matching conditions at the interface of the two layers, she obtained an equation similar to the Korteweg-de Vries equation for the upper layer. No exact solution of the resulting equation has been obtained, except for the case of a steady wave. The general shape of the steady solution is very similar to that of the classical solitary wave. Furthermore, a numerical solution of the Korteweg-DeVries equation by Zabusky and Kruskal (1965) resulted in a train of solitary waves similar to the waves observed by Gargett in Georgia Strait. For this reason, and also because of the close resemblance of her equation to the Korteweg-DeVries equation, she developed a non-steady solution, for a particular class of initial conditions (harmonic functions). The asymptotic behaviour of the two solutions was similar. For this special class of solutions, the initial wave form steepens in regions of negative slope, followed by the development of an increasing number of waves behind each steepened "leading edge". Each wave finally achieves a limiting amplitude, and then moves at a speed proportional to its amplitude, such that waves of a group slowly separate, with the largest amplitude waves leading.

As previously mentioned, Lee and Beardsley (1974) examined a similar non-linear theory to explain the behaviour of internal waves observed by Halpern (1971) in Massachusetts Bay. Following Benjamin (1966) and Benney (1966), they developed a time-dependent model (with a basic shear) that separated the influence of the non-linear, dispersive and non-Boussineq effects, by using a three-parameter perturbation expansion method. They computed numerically the values of these parameters from certain cases and compared their solution of the

Korteweg-deVries equation to the field observations of Halpern and their own observations in a small laboratory model. Their main conclusion was that a warm front in typical summer oceanic conditions will steepen and long non-linear internal wave trains will be generated on this depression owing to the dispersive effect of the sharp front. The properties of the front and the following waves are dependent upon the particular density and velocity profiles, as they control the dispersive and non-linear effects of the water.

2.4 DECAY

As noted in the preceding section, a small amplitude linear internal wave in a shear region will have a constantly changing frequency, wavelength, amplitude and direction of propagation. Because of these changes, the wave energy is also altered. The mean kinetic energy density of the wave motion is (Phillips, 1966):

$$E_K = \tfrac{1}{4}\rho_0 G^2(1+\beta^2 t^2 \cos^2\phi)^{-\frac{1}{2}}$$

Thus, E_K diminishes as the motion vanishes, for $\beta t \cos\phi \to \infty$. The energy loss is compensated by a small energy gain in the mean flow (Phillips, 1966).

One way for the wave to lose its energy is by decaying (partially or totally) into turbulence where the shear is maximum. For an internal wave, local instabilities occur near the trough and the crest giving rise to a patch of intense, small-scale turbulence. This occurs when the amplitude of the wave becomes sufficiently large. Each time this 'breaking' phenomenon occurs the wave loses energy and thus its amplitude is limited to a certain magnitude. Phillips (1966) comments on the consequences of this decaying:

> "It provides a means for the mixing of the fluid in the thermocline below the region of direct action of the surface layer. It is self-limiting; if a breakdown occurs, the subsequent turbulent mixing ultimately reduces the mean density gradient and decreases $N_{maximum}$ so that the condition for stability is restored (even if the wave slope is maintained) and the breakdown will tend to stop. The occurrence of the turbulent patches is therefore sporadic in space and time." (p. 187)

Another kind of turbulence was observed experimentally by Long (1955). In several of his pictures, taken of the flow behind an obstacle, one can see a patch of turbulence near the bottom under the first crest of the wave. Long related this turbulence to boundary layer separation. Since the turbulence is only present close to the barrier it is of no importance except to transfer a certain amount of energy from the waves to the flow.

One should also consider the dissipative effects present in any real physical environment that could rapidly damp any oscillation (see McIntyre, 1972). It is important to note that the wave will lose energy to the mean flow even in the absence of any dissipative effects.

In summary, a vertical oscillation in a fluid having a diffuse pycnocline, with a weak vertical shear, will become more and more horizontal; its amplitude, wavelength and frequency will diminish constantly and the wave motion, if not completely decayed to turbulence, will ultimately lose all of its energy and disappear.

CHAPTER 3

GENERAL CIRCULATION IN THE AREA OF STUDY

3.1 DESCRIPTION

The St. Lawrence river system extends from the Atlantic Ocean on the east coast of Canada to the Great Lakes, 1200 km inland. It is divided into four parts: (i) the fresh water river, (ii) the middle estuary, (iii) the maritime estuary, and (iv) the gulf.

The region of major interest in the present work is the middle estuary which extends from Ile d'Orléans (near Quebec City) to Tadoussac (see Figure 3.1) and can be classified as a "well-mixed" body of water. In this section there are many small tributaries that flow into the St. Lawrence. Only the Saguenay River, located at the downstream end of the middle estuary, is of sufficient size to significantly influence the water characteristics.

The most important bathymetric feature of the St. Lawrence estuary is the deep Laurentian channel, which extends from the Sagenuay River to the Atlantic Ocean. Upstream of Pointe des Monts, a shallow plateau can be found on the southern side. From Tadoussac to Pointe-au-Pic, a basin and sill configuration is found on the north side and a shallow plateau to the south. Upstream of this sill the river is quite shallow.

The focus of the present work is on a 40 km section of the middle estuary near Pointe-au-Pic, which is some 120 km

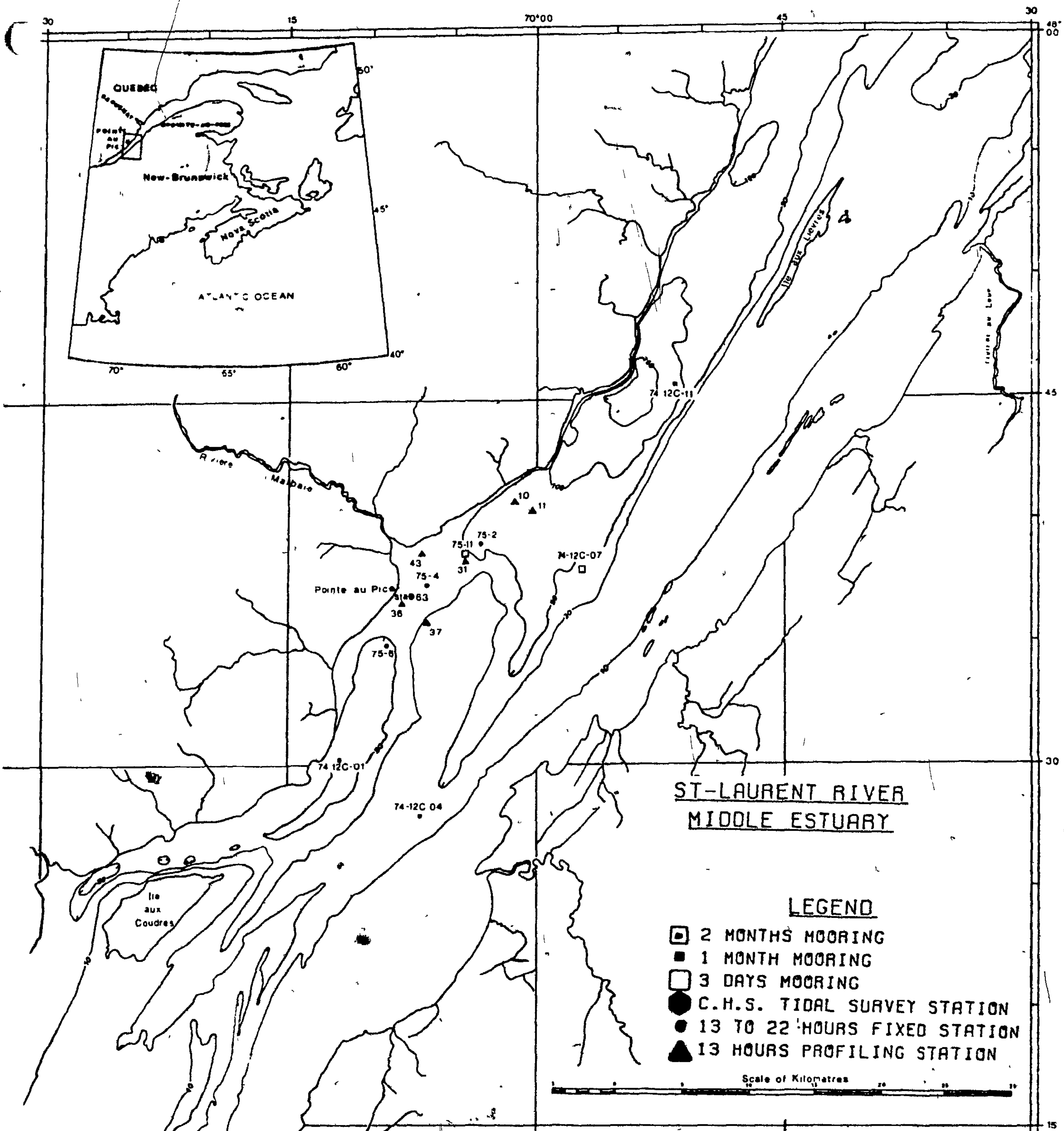

FIGURE 3.1 THE AREA OF STUDY

downstream from Québec City. At this point of the estuary, a large bank ("English Bank") partially obstructs the north side of the river, leaving a 6 km wide passage for the water to flow between the bank and the mainland. It was in this narrow passage that we hoped to observe internal waves.

In Figure 3.2, which shows the bottom topography of this region, a curved line passing through several stations is also plotted. A bathymetric section along this line can be found in Figure 3.3. It shows the profile of the English Bank and the relative position of the principal measuring stations. It should be noted that the vertical scale of this section is exaggerated (185 times) compared to the horizontal scale. Thus, in reality, the bank is just a gradual change in the depth of the river. Even so, this natural obstacle to the prolongation of the north channel appeared to be a suitable area in which to observe topographically induced internal waves.

To understand the behaviour of the internal waves and to have a general idea of the circulation in this region, three properties were measured: the currents, the vertical gradient of the horizontal velocity (shear) and the density (instantaneous profiles and time series at a constant depth). The following sections of this chapter present these results and also provide a description of the general oceanography in this part of the middle estuary during the summer.

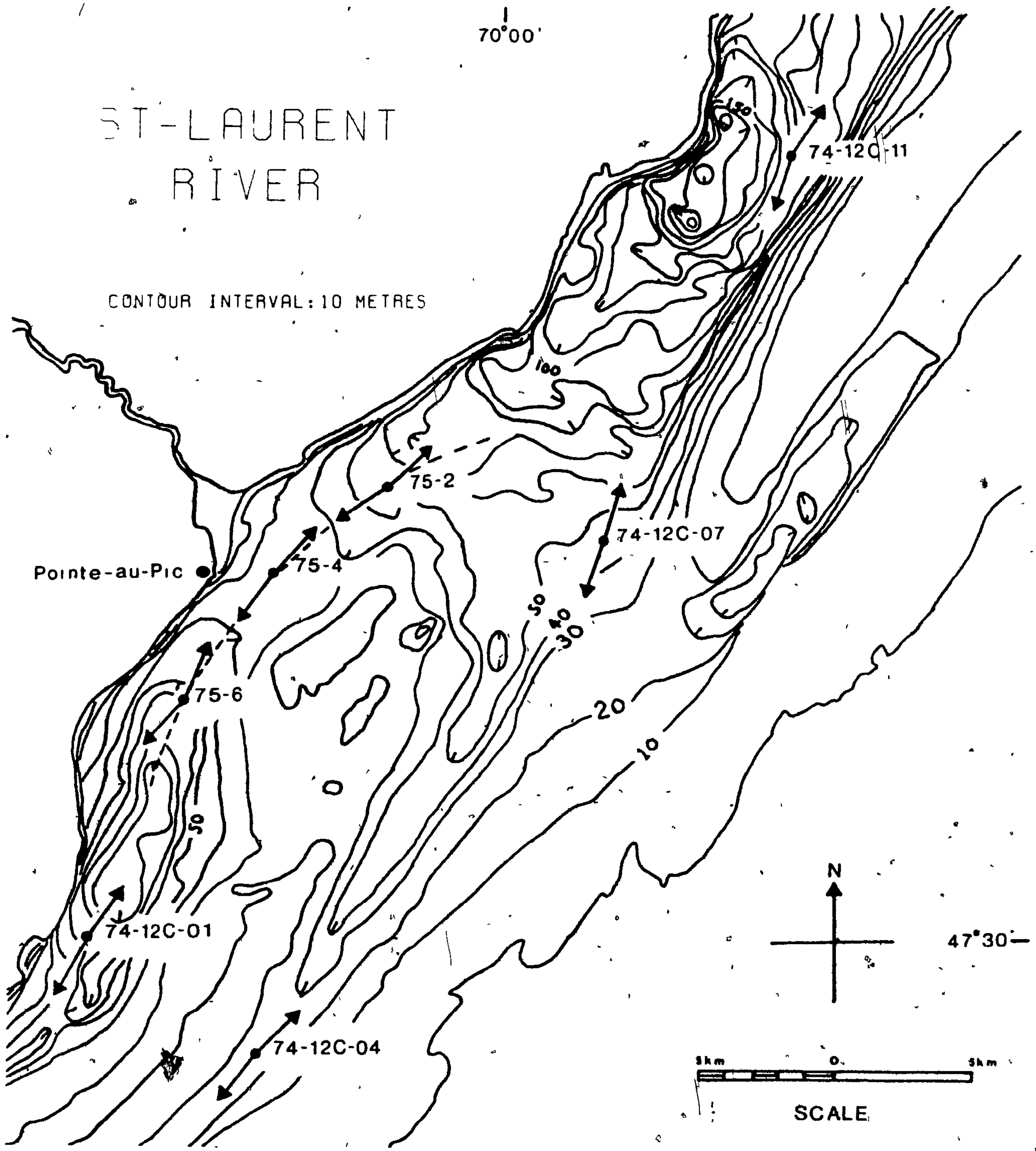

FIGURE 3.2 BATHYMETRIC CHART OF THE REGION AND AVERAGED TIDAL CIRCULATION

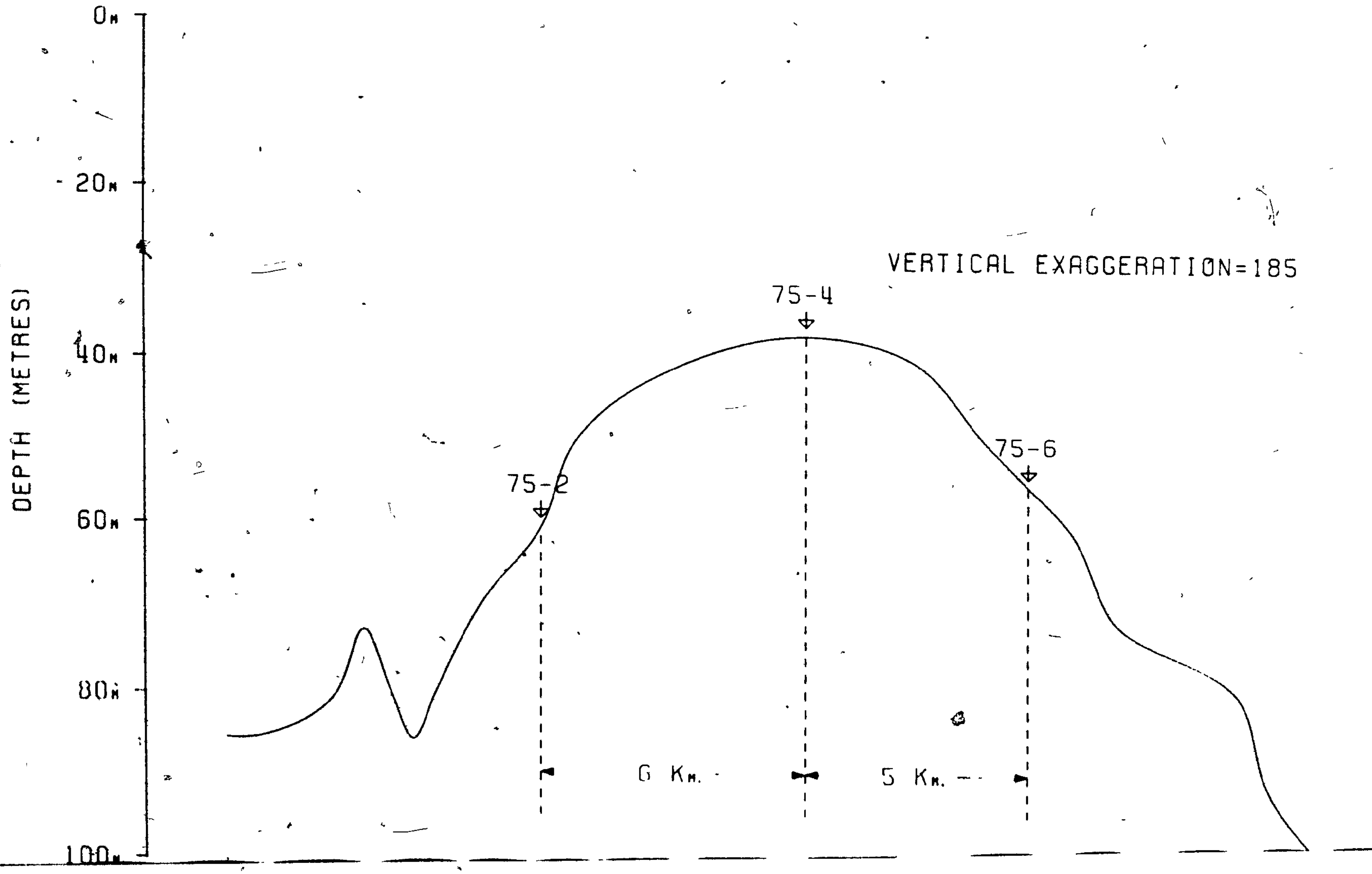

FIGURE 3.3 LONGITUDINAL SECTION OF THE BOTTOM IN THE STUDY AREA

3.2 CURRENTS

In describing the circulation of this region, two sources of information were used: current meter data obtained from an unpublished report by the Canadian Centre for Inland Waters (CCIW) (Budgel and Muir, 1975), and data taken personally in June and July 1975 (at stations numbered 75-2, 75-4, 75-6 and 75-11). Station position is shown in Figure 3.1, while the exact location is given in Appendix 1.

Current meter data were obtained during two cruises. On the first occasion the current was measured at a fixed depth for 13 hours at three stations (sampling interval = 30 sec). During the second cruise, currents were recorded at the same locations over a similar interval of time but at different depths. Although measurements should have been taken at the same depths on both cruises, this did not occur for reasons explained in Chapter 4.

These data, taken at different depths and on different days, were not overly useful in their original form, but required a certain readjustment in time before comparison. Instead of using local time as a reference for when measurements were taken, the most appropriate time reference available was the tidal predictions of the

Canadian Hydrographic Service (hereafter called CHS) (1975) for the nearest reference port, which is Pointe-au-Père (see Appendix 2). By combining all our observations at different depths and different times relative to the predicted tides at Pointe-au-Père, a general picture of tidal currents in this area can be obtained. Figures 3.4, 3.5 and 3.6 show these results at the three main stations.

In these diagrams, tidal currents are represented by vectors pointing in the direction in which the current is flowing relative to true North (top of the page), while the overall length of the centered arrow is proportional to the speed of the current. The magnitude was calculated from a vector average of 120 values observed over a one hour period, centered on the appropriate tidal phase. During times of rapidly varying current direction (as when the tide is turning at slack), the average speed is shown instead of an arrow.

Also calculated were $\overline{U}_{depth}$ and $\overline{\theta}_{depth}$, which represent the depth-averaged current vector, computed (scalar average) over the appropriate water column height. These are shown under the last depth recorded for every hour of the semi-diurnal tidal cycle. Also shown is the semi-diurnal tidal average (vector) at each depth, $< U, \theta >$.

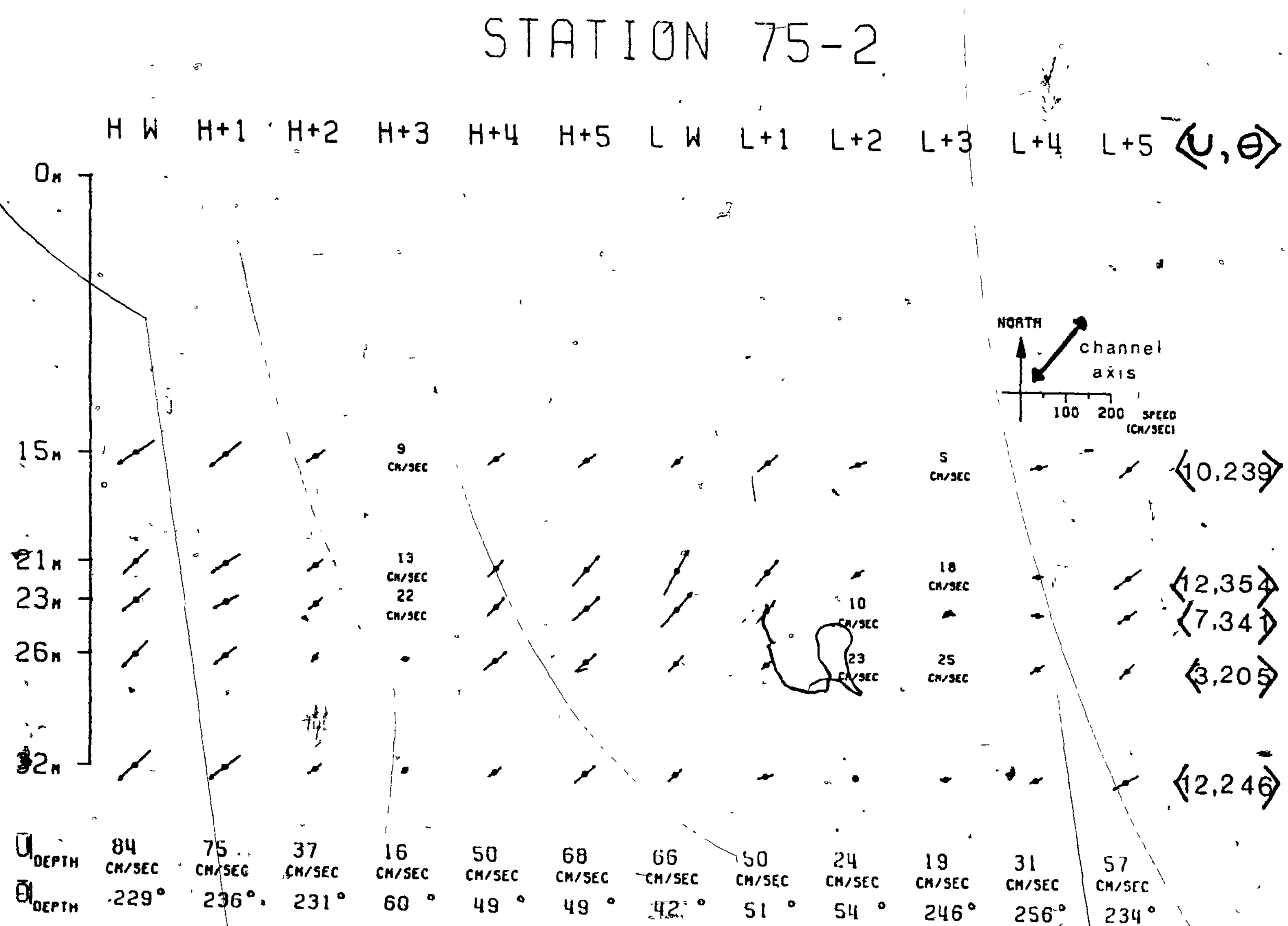

FIGURE 3.4 TIDAL CURRENT DISTRIBUTION

STATION 75-4

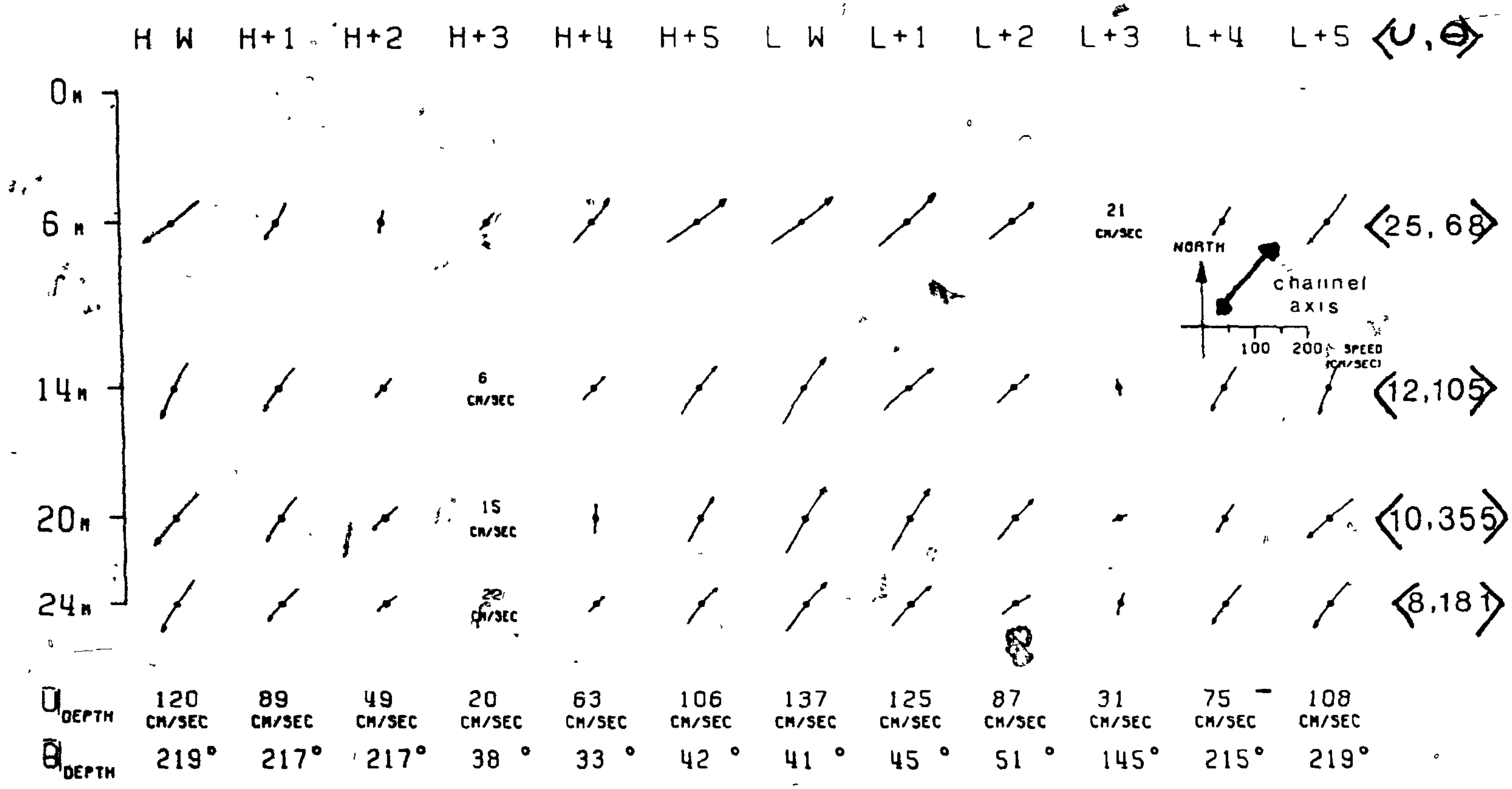

FIGURE 3.5 TIDAL CURRENT DISTRIBUTION

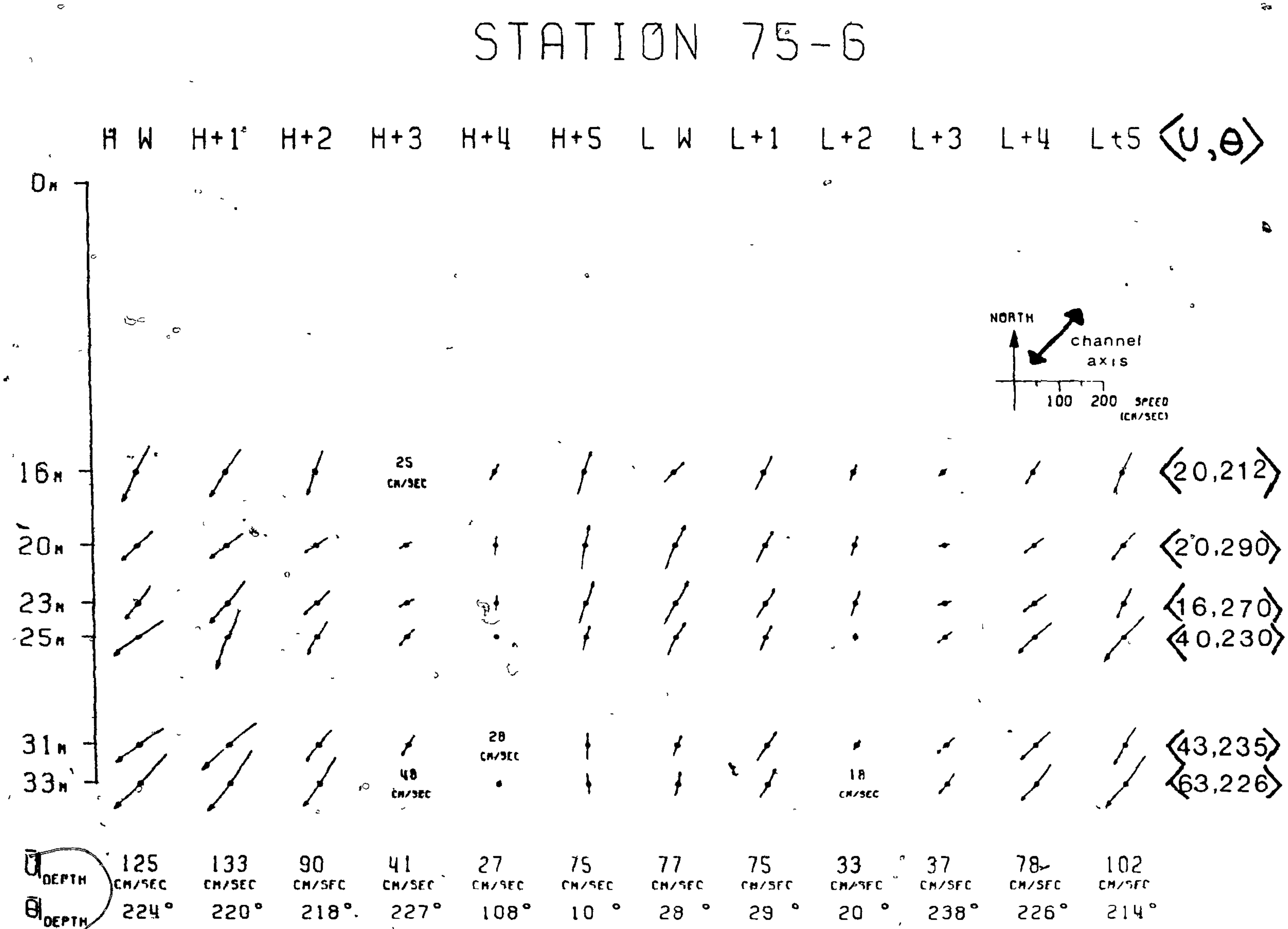

FIGURE 3.6 TIDAL CURRENT DISTRIBUTION

Included in Figure 3.5 are the current vectors obtained by CHS (1939) at a depth of 6 m for their station 63. These data were taken in surveys during the mid-1930's. Station 63 was the only one close enough to the region of the present study to be of interest.

From Figures 3.4, 3.5 and 3.6 it can be seen that the water turns, slack water, 2 to 3 hours after the predicted time of low tide at Pointe-au-Père and 3 to 4 hours after the predicted high water, in agreement with CHS (1939) results.

The CCIW report includes data obtained from moored current meters at four different locations in the summer of 1974. Their stations are those numbered with "74" prefix in Figure 3.1. Average directions at these stations are computed and shown in a histogram form on Figures 3.7, 3.8, 3.9 and 3.10. These diagrams will be used in conjunction with our own observations to map the general circulation in this region. Note that the mooring at station 74-12c-07 lasted for two months whereas the other stations were held for approximately one month.

One of the ways to illustrate the circulation in this part of the middle estuary is to plot the direction of the ebb and flood at many differing locations. Mean ebb and flood directions at the CCIW stations

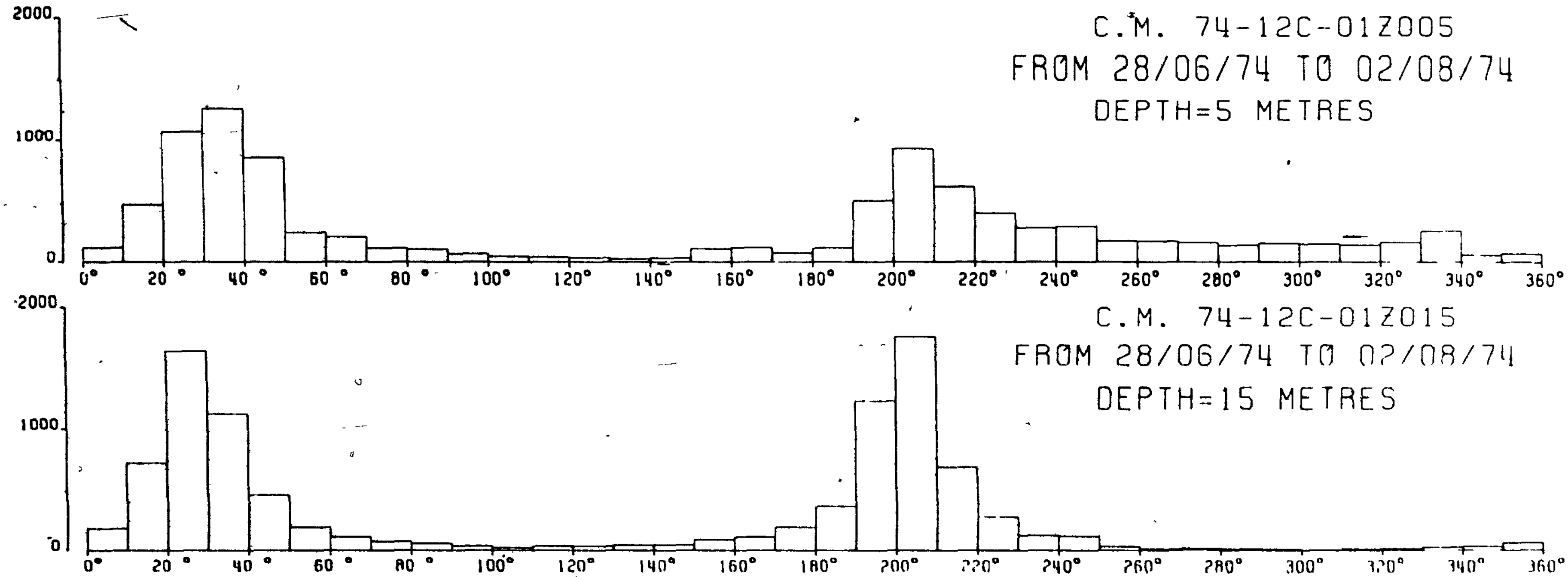

FIGURE 3.7 DIRECTION HISTOGRAMS

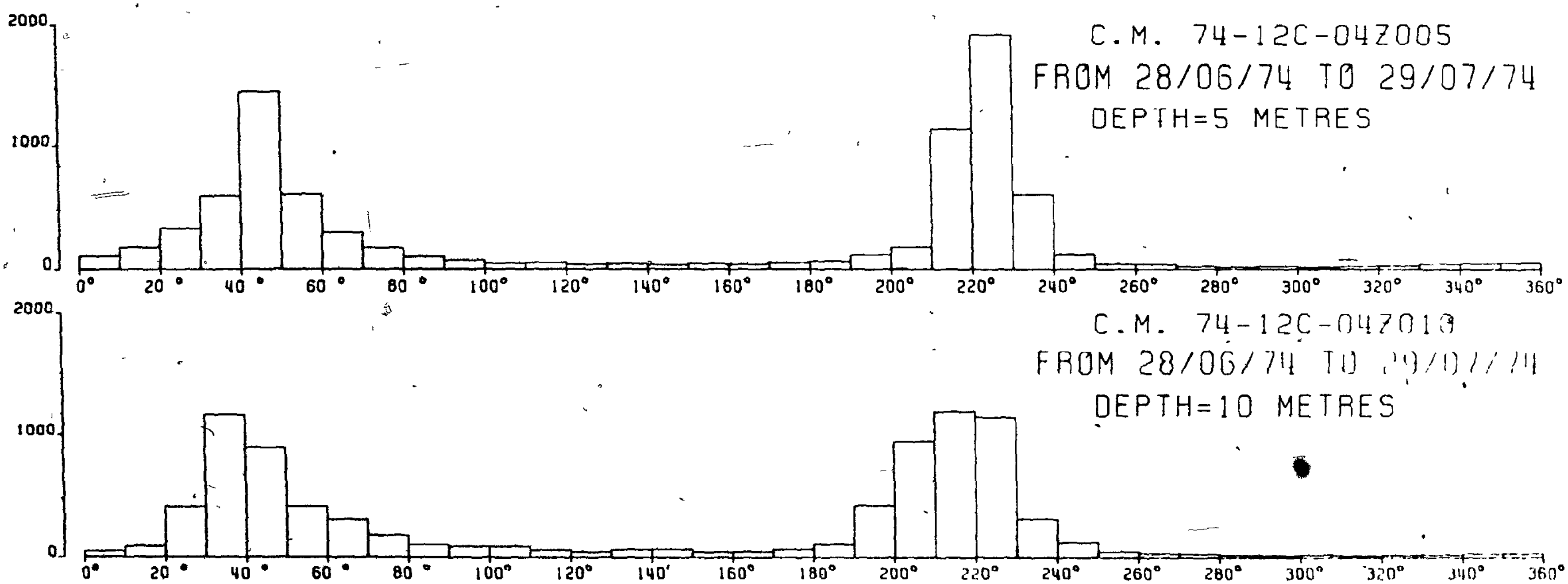

FIGURE 3.8 DIRECTION HISTOGRAMS

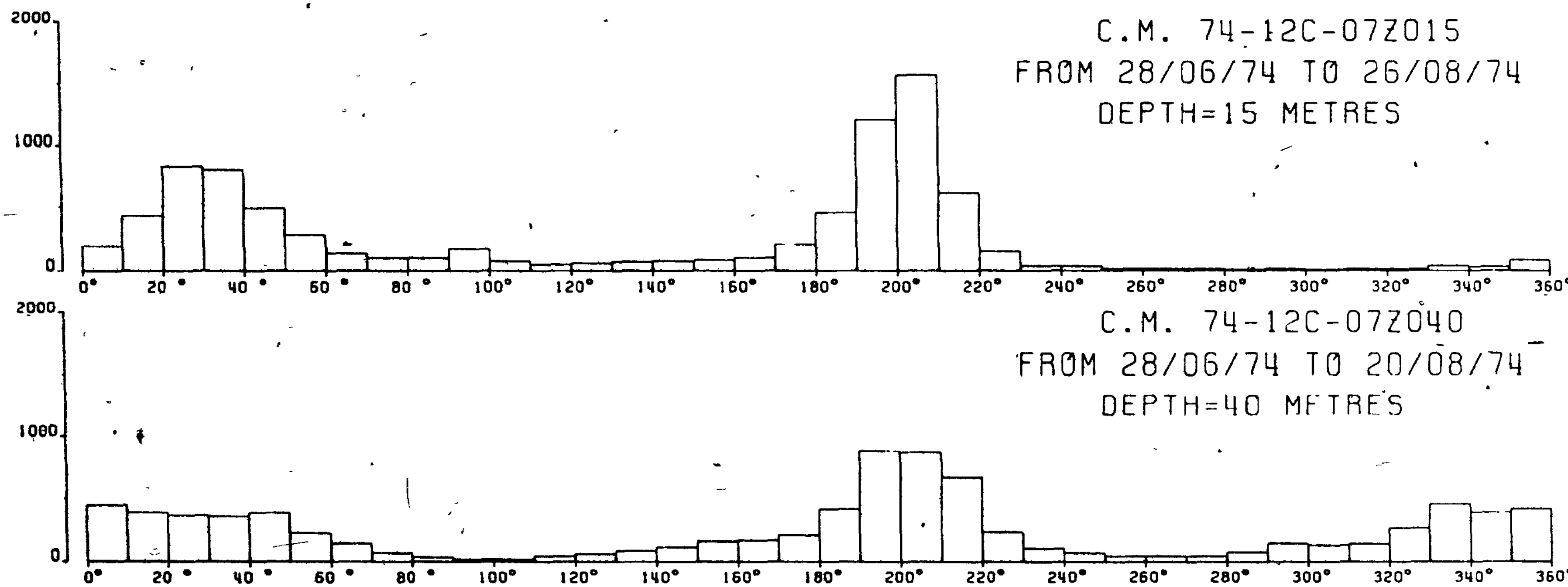

FIGURE 3.9 DIRECTION HISTOGRAMS

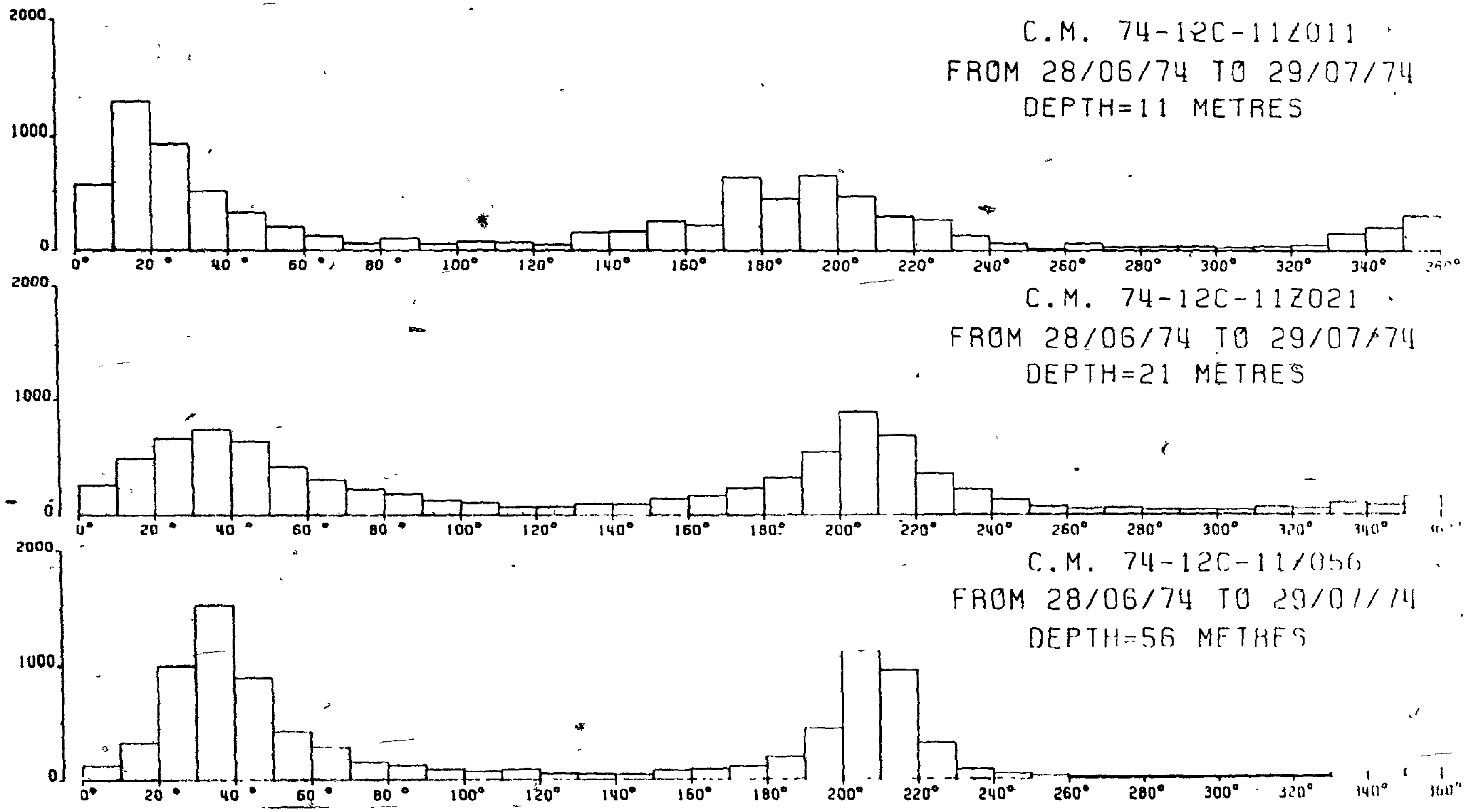

FIGURE 3.10 DIRECTION HISTOGRAMS

and at those of the present study are listed in Table 3.1.

Station	Ebb	Flood
74-12c-01	32^{0}	209^{0}
74-12c-04	45^{0}	219^{0}
74-12c-07	17^{0}	199^{0}
74-12c-11	32^{0}	199^{0}
75-2	48^{0}	237^{0}
75-4	42^{0}	217^{0}
75-6	22^{0}	224^{0}

TABLE 3.1: AVERAGE EBB AND FLOOD DIRECTION

These averages were obtained from direction histograms at one or more depths and over a one or two month period for the CCIW data and 13 hour intervals for the remaining data. The information shown in Table 3.1 has been summarized in Figure 3.2 as two arrows representing mean ebb and flood directions at each station. The length of the arrows is not proprtional to the current magnitude. Plotting the data in this manner is useful, in that it shows how the water flows on each side of the English Bank.

3.3 VERTICAL SHEAR

As explained in Chapter 2, any discussion of internal wave generation or their properties requires knowledge of the local velocity shear. In the present case, only the vertical shear of the horizontal velocity field can be calculated. These considerations are useful, since internal waves behave differently in a "strong" or a "weak" shear. To differentiate between these two cases an argument based on the gravitational stability (Richardson number) of the water column will be employed.

Unfortunately, velocity shear over the complete water column was not measured routinely during the cruises. In order to estimate shear values in the region, current profiles from the CCIW report were used. They obtained a large number of current profiles with an Endeco model 110 direct readout current meter at each one-tenth fraction of depth. Samples were taken every forty-five minutes over a period of thirteen hours. The station locations do not exactly coincide with those of the present study but are usually close enough to be representative of the area.

The shear $\beta = \left|\frac{\partial U}{\partial z}\right| = \left\{\left(\frac{\partial u}{\partial z}\right)^2 + \left(\frac{\partial v}{\partial z}\right)^2\right\}^{1/2}$ where $U = U\ (u, v)$

was computed at different depths from the individual velocity profiles taken at their stations 10, 11, 31, 36, 37 and 43 (Figure 3.1). These shears were scalar averaged over 13 hours at every depth and plotted in Figure 3.11, 3.12 and 3.13. Graphs of adjacent stations are grouped together on the same figure. The mean shear (the simple average of the individual values plotted) and the total depth are given with the station number. From these graphs it can be seen that the mean shear never exceeds 0.1 sec^{-1}) ($\frac{\partial u}{\partial z}$ being the more important term of β). With this value, an argument similar to that used by Phillips (1966) can be employed to determine the importance of shear on the internal wave properties.

It is generally accepted that a local Richardson number larger than 0.25 is a sufficient criterion for the existence of stable internal waves (see Howard (1961) and Miles (1963)). Considering that characteristic values of the Brunt-Väisälä frequency, N, in the region during June and July 1975 varied from 10^{-2} sec^{-1} to 10^{-1} sec^{-1}, the local Richardson number, J, can be calculated:

$$J = \frac{N^2}{\beta^2}.$$

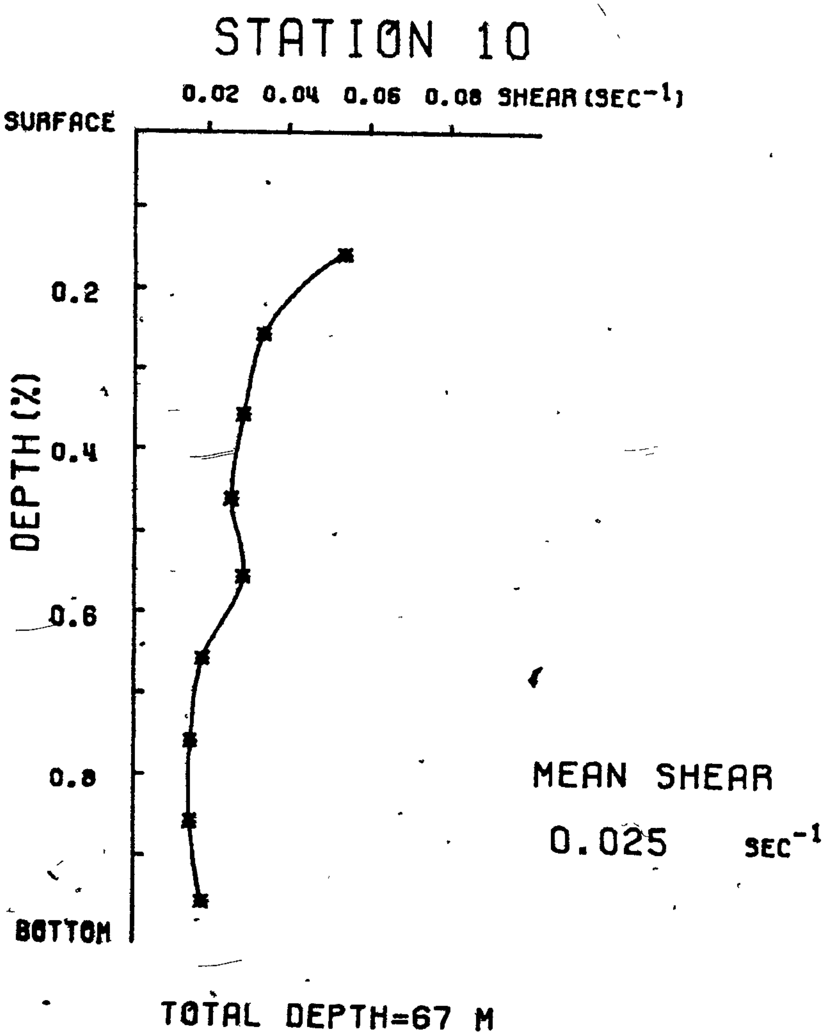

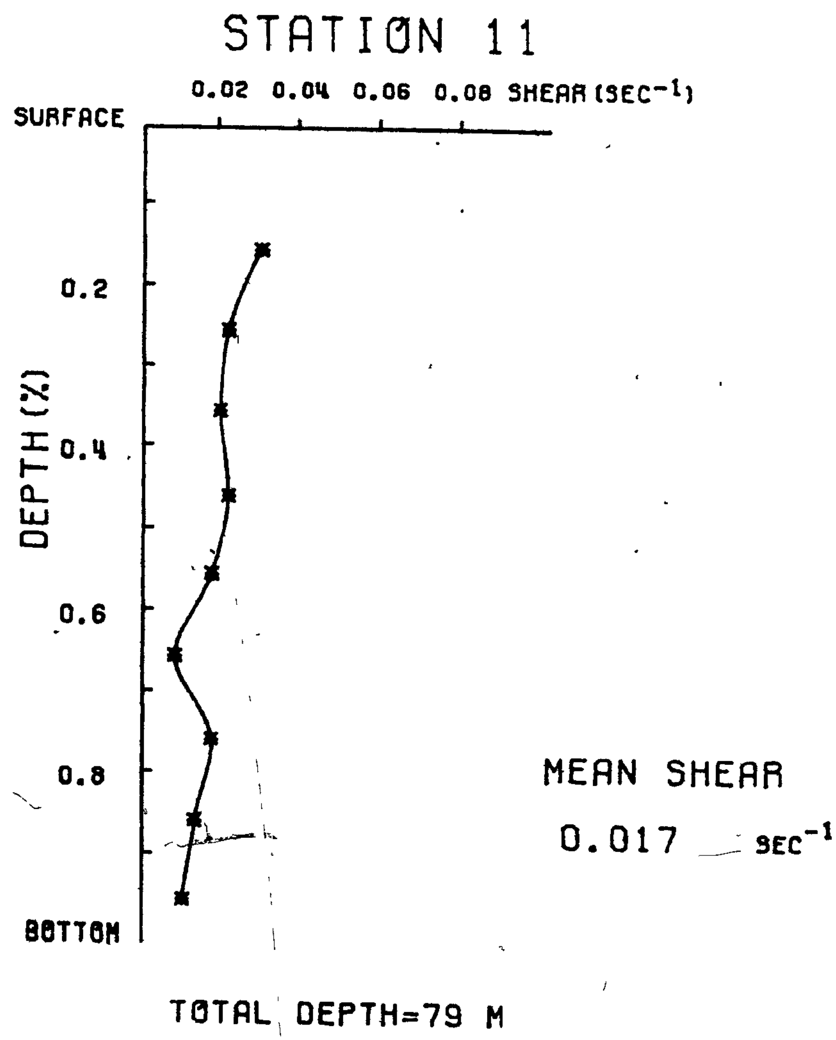

FIGURE 3.11 VELOCITY SHEARS

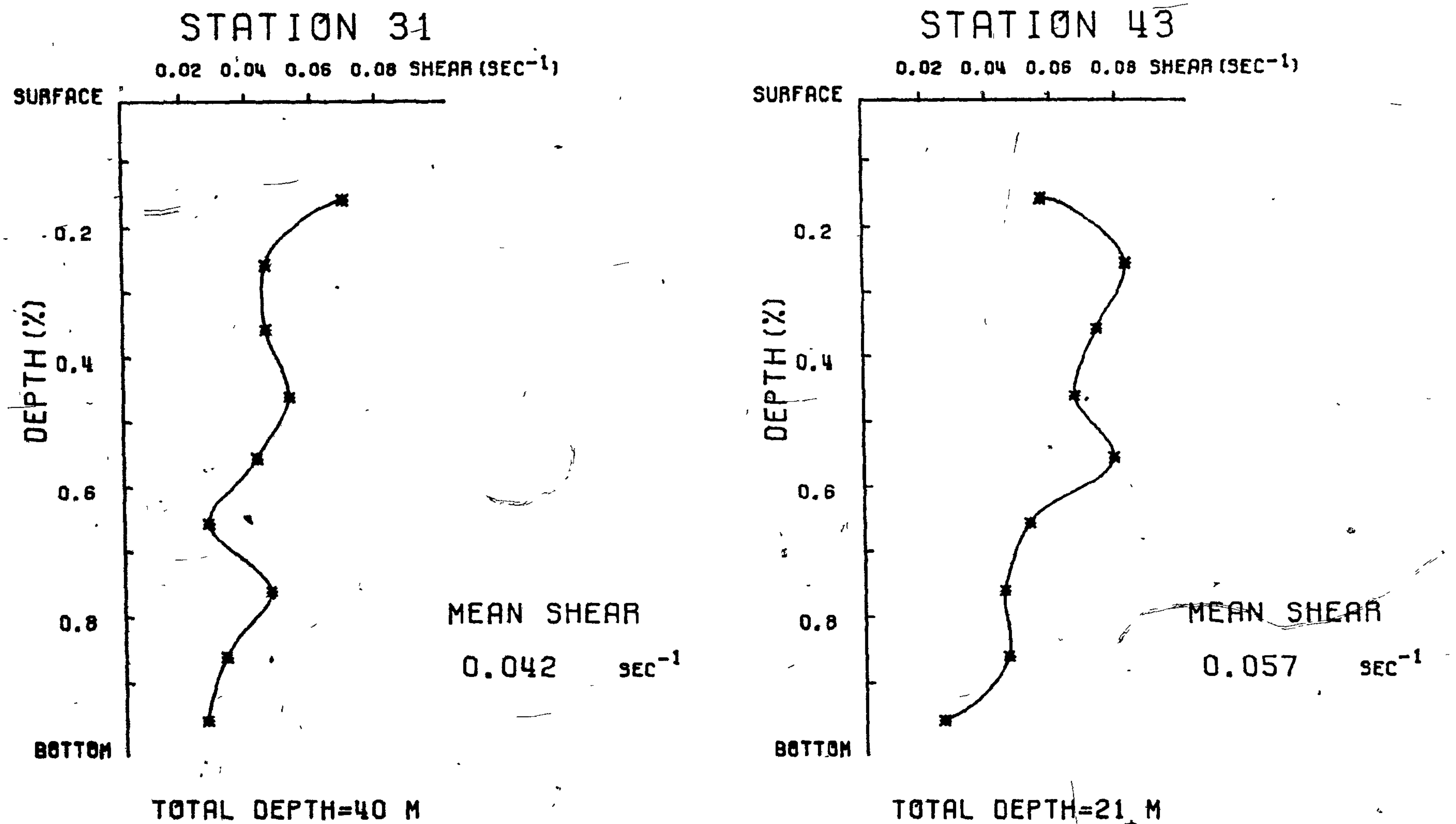

FIGURE 3.12 VELOCITY SHEARS

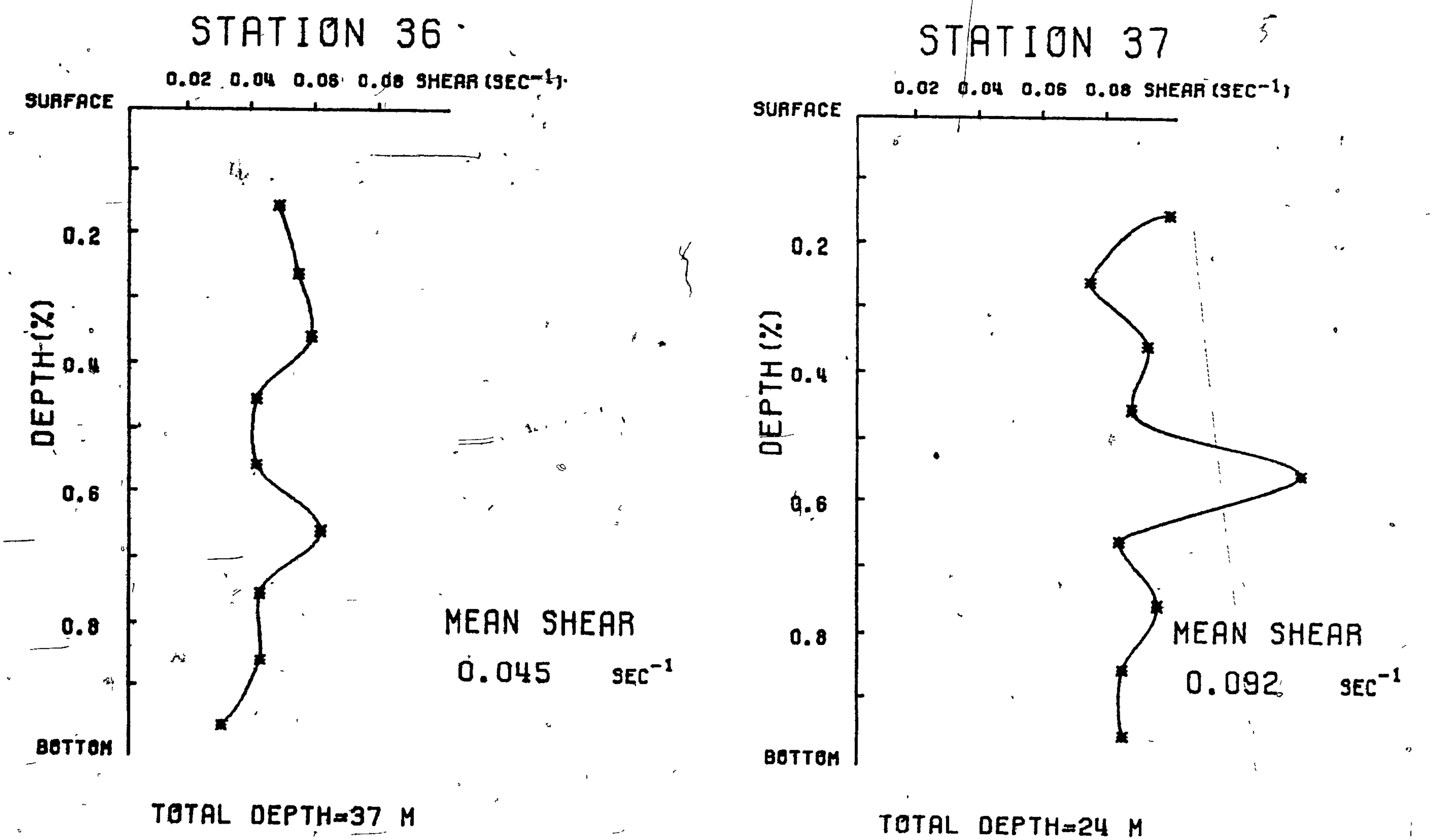

FIGURE 3.13 VELOCITY SHEARS

For the least stable case ($N = 10^{-2}$ sec^{-1}), $\beta < 2\ N_{max}$, or $\beta < 0.02$ sec^{-1} is an upper limit on shear for the existence of small amplitude internal waves.

In the present case, it is difficult to say if the shear was "small" or "large". Values of N which were used represent a large range and are not actual values measured simultaneously with the vertical shear (β) and the wave properties. Also, shear values presented in Figures 3.11, 3.12 and 3.13 are subject to a large variance (50% to 70%) and are based on data collected a year before the actual study. Thus, without an exact and simultaneous measure of N and β, it is not possible to determine if J is smaller or larger than 0.25 for each case.

3.4 DENSITY

Density information came from STD profiles taken hourly (more or less) at three stations: 75-2, 75-4 and 75-6, in the summer of 1975. In a similar manner to the current records, the observations will be related to a common reference, namely the tidal prediction at Pointe-au-Père. Assuming that density changes are linear in time between hourly profiles, an interpolated density profile can be calculated at any particular time in the tidal cycle. The values shown in Figures 3.14, 3.15 and 3.16 have been computed in this manner. All densities are in σ_t units. The assumption of linearity between profiles does not hold in all cases.

Except at station 75-6, profiles are regular and with no evidence of rapid change in density. For most cases, density varies linearly with depth below 20 m. By combining the information contained in these three figures the two-dimensional pattern of the isopycnal lines between stations at each hour of the tidal cycle can be calculated (Figure 3.17). It is not surprising to expect the bathymetry of the region to have an influence on the shape of these lines. The bank seems to act as a barrier (especially at high tide), preventing denser bottom water ($\sigma_t \geq 23$) from going further up the river, so that density is always higher on the downstream side of the sill.

Also of interest is the distinctive shape of the isopycnals at ebb and flood: almost straight (or even concave) at ebb, they become convex at flood, following the shape of the bank. This can be explained when we consider that the denser water carried from the downstream side probably sinks under the fresher water on the upstream side, after passing the obstacle at flood. At ebb, the opposite phenomenon occurs, with the fresher water sliding over the denser

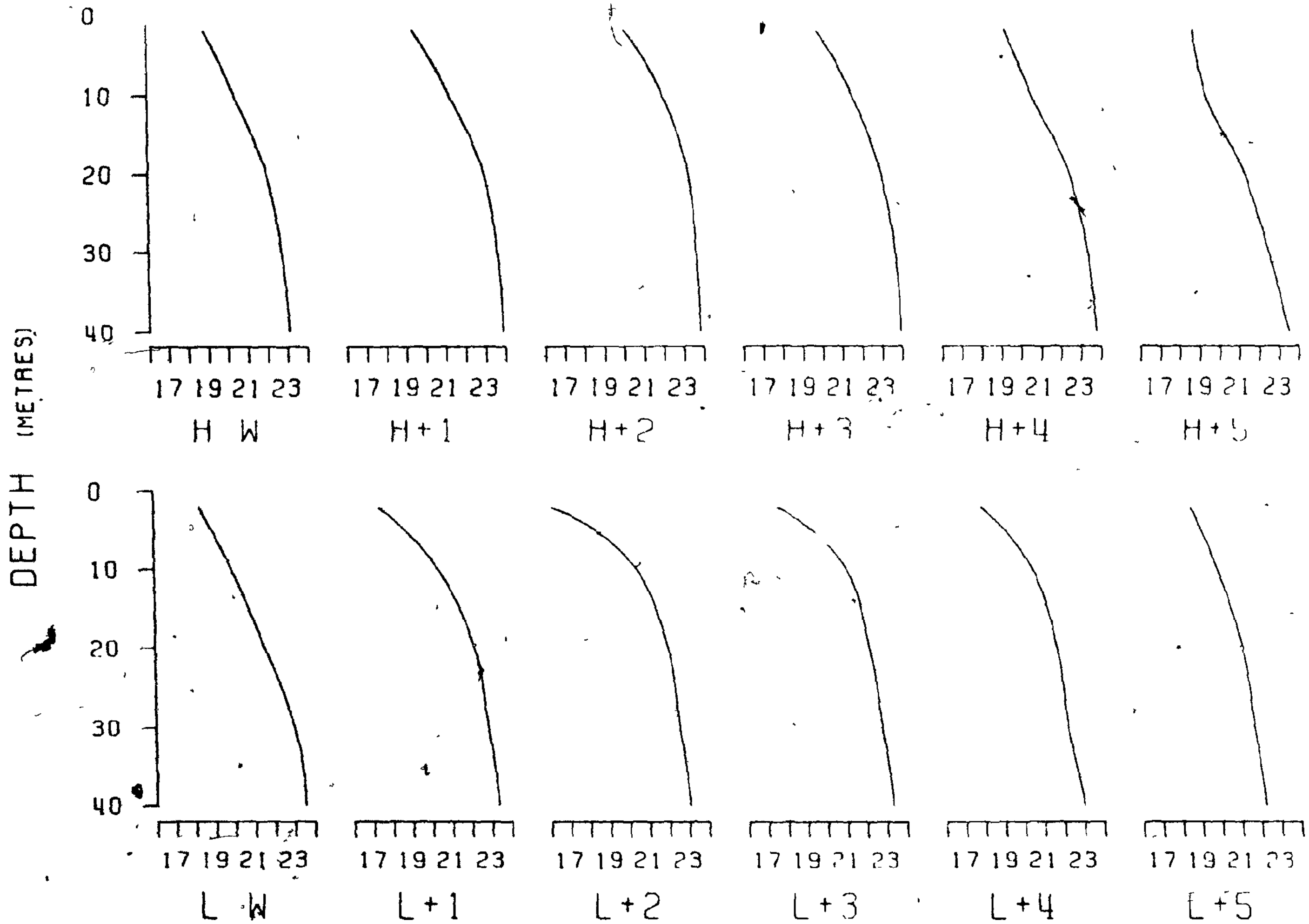

FIGURE 3.14 SIGMA-T PROFILES AT 75-2

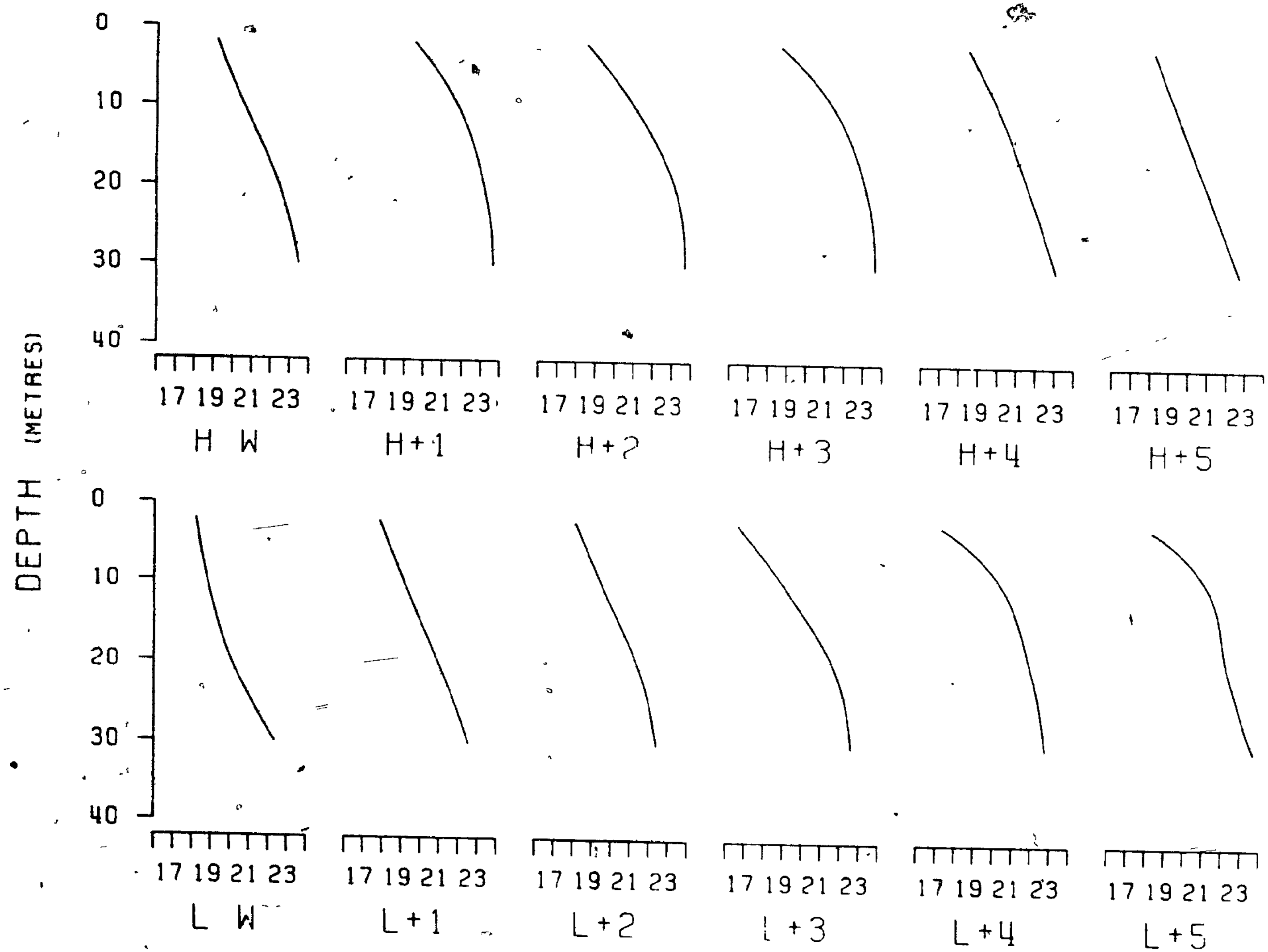

FIGURE 3.15 SIGMA-T PROFILES AT 75-4

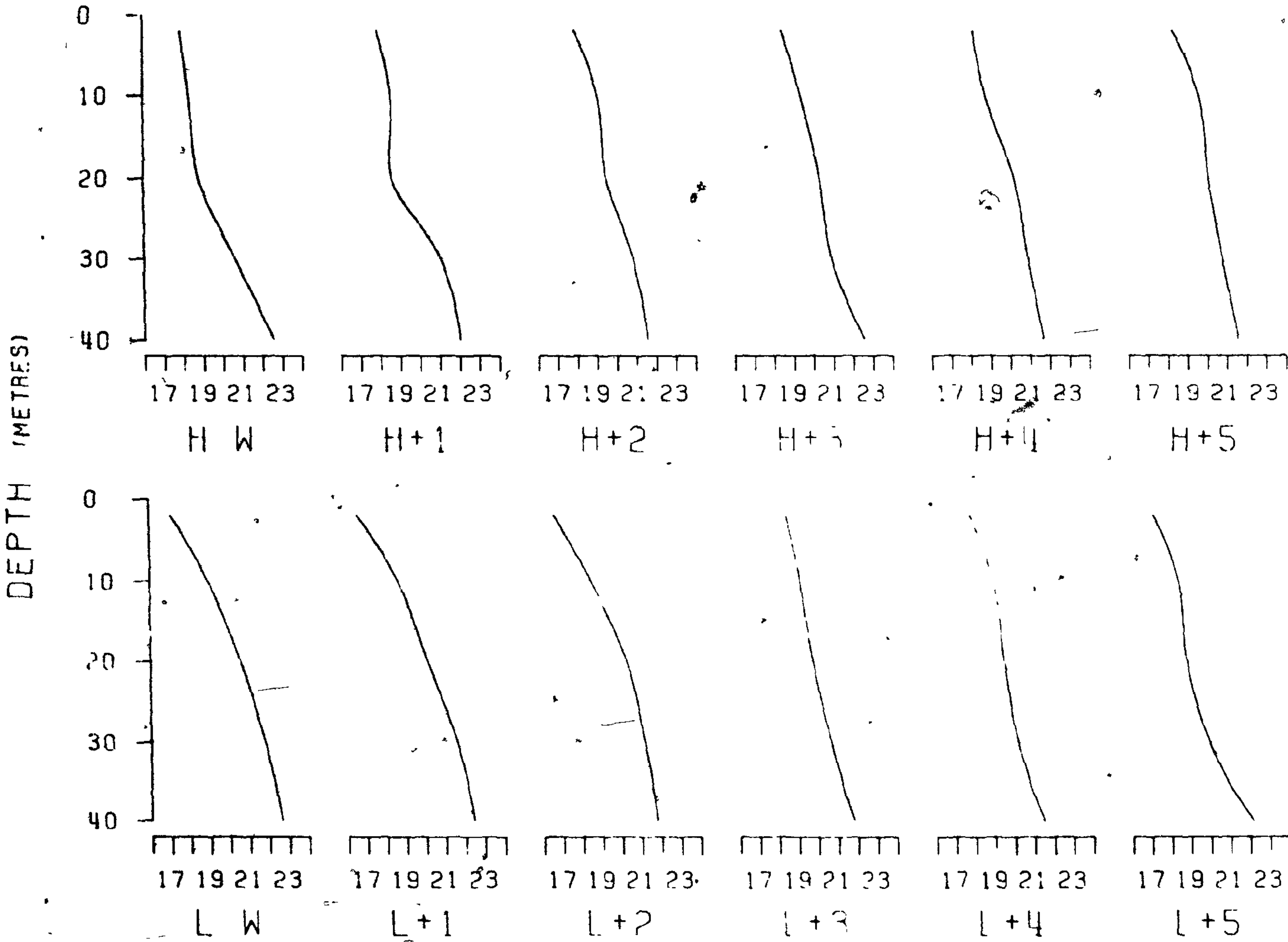

FIGURE 3.16 SIGMA-T PROFILES AT 75-6

water on the downstream side of the sill.

The vertical spacing between density lines in Figure 3.17 differs on each side of the bank: near station 75-6, probably due to the depression lying at the base of the sill in this area (see Figures 3.1 and 3.2), the isopycnals are more widely separated (especially at slack water) than near station 75-2. Greater spacing between isopycnal lines implies a smaller density gradient or less stability over the water column.

These two properties of the isopycnals can be used to explain why the density profiles at station 75-6 are more irregular than at the other two sites. At flood (L + 5 → H + 2), when the heavy water sinks under the fresh after being pushed over the bank by the tide, a stronger pycnocline (a region of sudden change in density) can be expected somewhere in the water column. At this stage of the tide we can see that the isopycnals are closer together due to this intrusion of saltier water, creating a more stable regime. When the tide goes out (H + 5 → L + 2) the water column becomes more homogeneous and less stable.

In addition to the STD profiles, time series of density were obtained from the salinity and temperature values recorded at fixed depths by the Aanderaa current meters. The sampling interval and

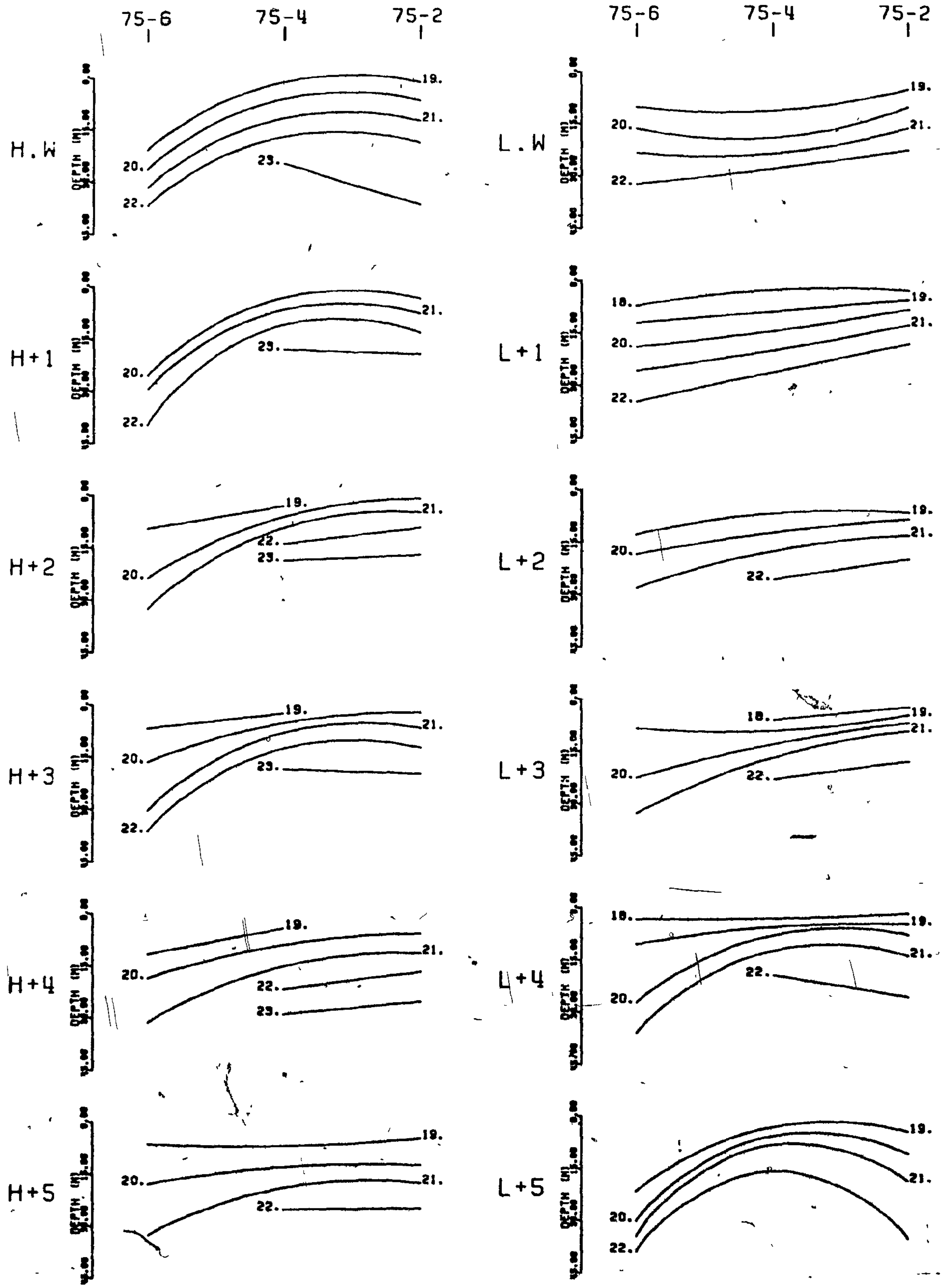

FIGURE 3.17 ISOPYCNAL LINES
(density in sigma t units)

response time of the instrument were 30 seconds and 1 second respectively, allowing observation of any high-frequency phenomena of period 1 minute or greater, with a precision limit of ±0.2 σ_t units. This error results from both digitization of the data and the sensor accuracy. These time series will be used extensively in Chapter 4.

A good example of density variation is given in Figure 3.18. This graph shows the density fluctuations at 30 m for mooring station 75-11 from 1215 EST July 22 to 0220 EST on July 25.

Part (a) is the complete three day record. For clarity, values of density have been smoothed by using the formula:

$$\sigma_{t_i} = \frac{\sum_{k=i-5}^{i+5} \sigma_{t_k}}{11}$$

The time interval between each point is 30 seconds. Parts (b), (c), (d), (e) and (f) present the same data as part (a) but this time unsmoothed and cut into exactly five semi-diurnal tidal cycles. The predicted times for high and low water at Pointe-au-Père are shown. Marks on the abscissa are tidal phases (in hours) between these low and high tides.

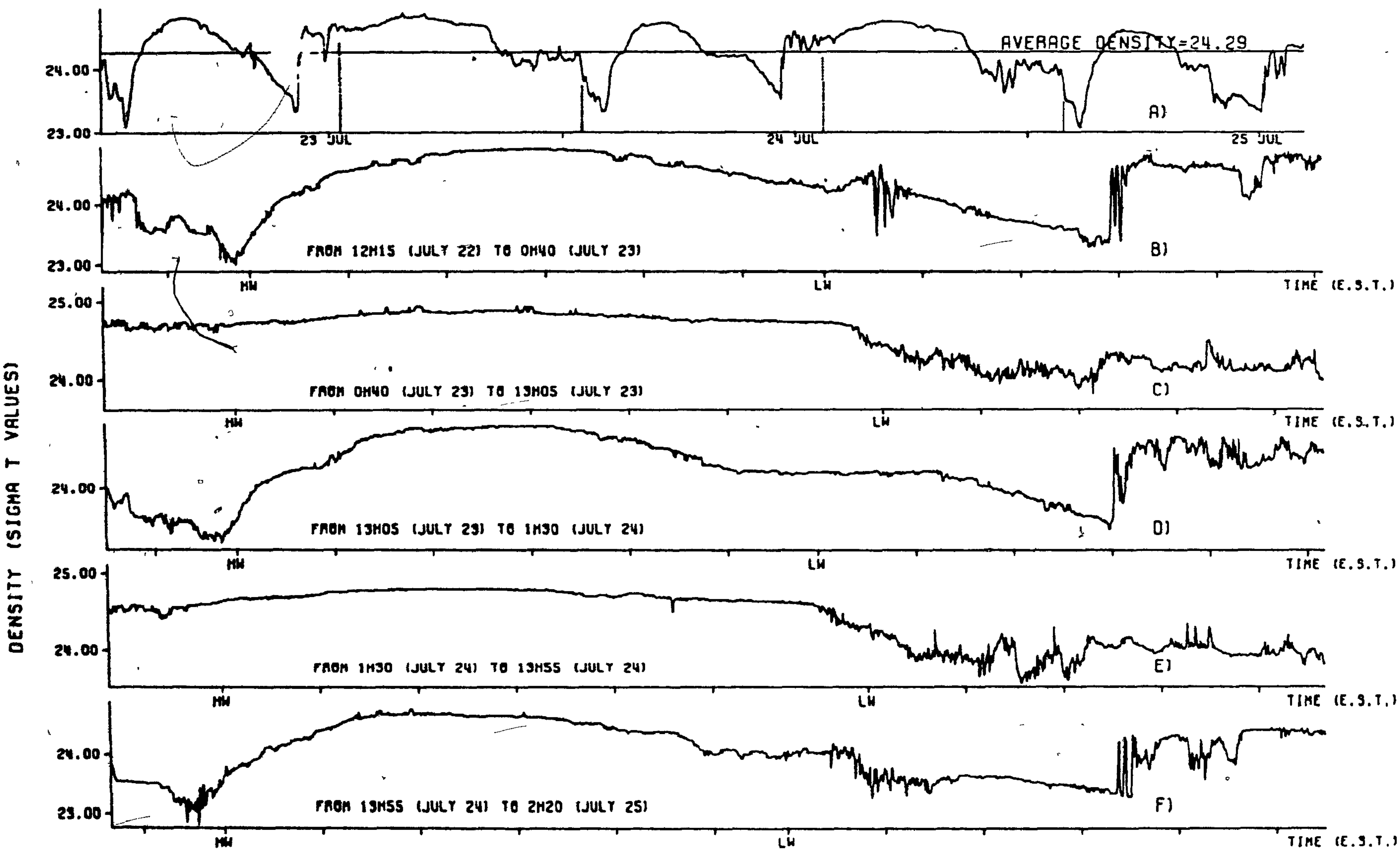

FIGURE 3.18 DENSITY VARIATIONS OVER THREE DAYS AT 75-11

Notice the striking repetition of the pattern every two cycles and the appearance of large amplitude, high-frequency fluctuations 3 hours after low water in parts (b), (d) and (f). The alternating pattern (diurnal) in part (a) of Figure 3.18 resulted from an asymmetry of sequential tidal waves. The abrupt increase in density observed every two tidal cycles seems to be of frontal origin, although the generation of these fronts remains unexplained. The appearance of large fluctuations of the density field may be related to the presence of this frontal phenomenon (Halpern, 1971).

Looking at Figure 3.18 reminds one to be careful in the interpretation of data recorded over a single tide cycle or with a long sampling period in this region. Since density values change by one or two σ_t units in five or ten minutes, data collected in hourly sampling programs in this area would be subject to considerable aliasing. Temporal variability is usually important in an estuary and great care should be taken to consider the high frequency changes of the water properties.

Prior to a consideration of internal waves, the main interest of this study, the main features of the circulation will be summarized.

During a twelve-hour interval, circulation in the small passage between Pointe-au-Pic and the English Bank is quite predictable. Slack occurs 2 to 3 hours after low tide and 3 to 4 hours after high tide at Pointe-au-Père. The maximum current recorded during the present survey was 180 cm/sec at a depth of 14 m (station 75-4). The flood was usually longer than ebb and the mean vertical shear was typically less than 0.1 sec^{-1}.

The range of densities over the water column, as obtained from Figures 3.14, 3.15 and 3.16, was 1.013 gm/cm^3 to 1.026 gm/cm^3, over a semi-diurnal tide cycle. Longer tidal period and seasonal density changes cannot be discussed using these records.

CHAPTER 4

INTERNAL WAVE OBSERVATIONS

4.1 EXPERIMENTAL LAY-OUT

Data were collected in the region of Pointe-au-Pic during two cruises on the 100 foot oceanographic vessel M/V METRIDIA. From 22-25 June and from 22-25 July 1975, three fixed stations (75-2, 75-4 and 75-6) were held, each for a period of time varying between 13 and 22 hours. In order to obtain space and time information on internal waves three Aanderaa current meters were used simultaneously: CM 1 and CM 2 were fixed, one over the other, on line 1 attached to the ship and CM 3 was on line 2 fixed under an ORE float a certain distance (44 m) behind the ship (see Figure 4.1). STD profiles were routinely taken from the ship.

From wavelength and phase velocity measurements obtained under similar conditions at a neighbouring location, it was decided to attach the supporting buoy 44 m behind the ship (approximately one-third the expected wavelength). As a result of the depth-dependent shear (especially near slack water) and because of the wind pushing the stern of the ship, the relative distance between the two lines was constantly varying, making precise determination of phase speed and wavelength very difficult.

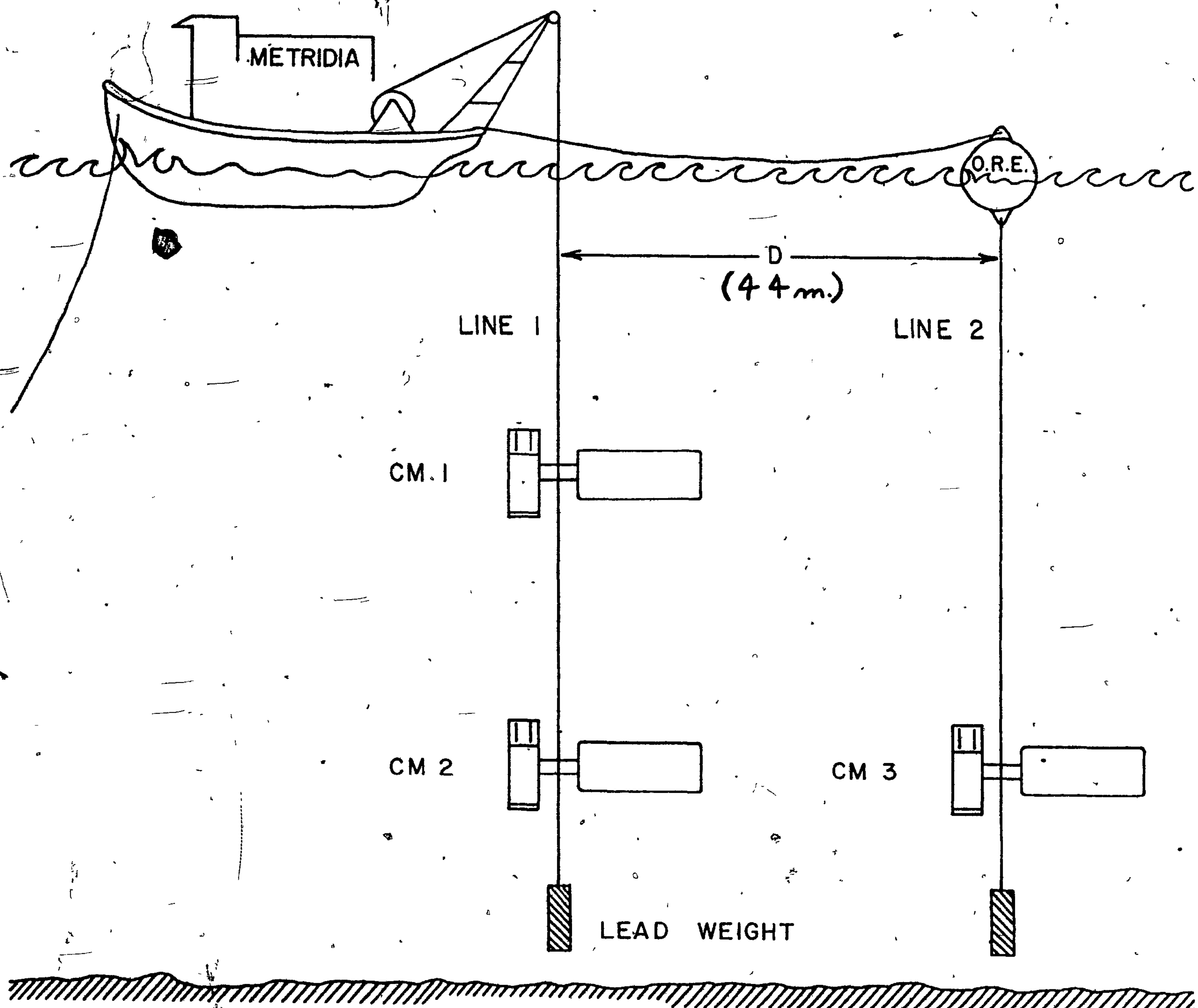

FIGURE 4.1 EXPERIMENTAL SET-UP

Another problem occurred due to the length of each line. The original idea was to keep CM 2 and CM 3 at the same depth, and CM 1 some 15 m higher. Unfortunately, this plan was not realized and in most cases the lower current meters were at slightly different depths.

During the second cruise a fourth Aanderaa current meter (30 sec sampling) was moored at station 75-11 in 43 m of water for a period of 3½ days.

4.2 EXPERIMENTAL RESULTS

From the two cruises, 17 current meter recordings of various length and numerous STD profiles were taken and analysed. Values of depth, salinity and temperature were used to calculate the density of the water every 30 seconds and STD profiles were used to plot graphs of density and of the BV frequency at various depths. Evidence of coherent, periodic density oscillations can be observed at least once on each of the 17 series obtained. A list of these occurrences and complementary information is compiled for every station in Tables 4.1, 4.2 and 4.3. Predicted tidal conditions at Pointe-au-Père are given with the time interval over which the oscillations are observed. The meaning of the underlining in the tables will be explained later in this section.

Station 75-2

CM	Depth (m)	From (EST)		To (EST)		Direction	Current (cm/sec)
1	15	11:39 (L+4)	June 23	13:44 (H.W.)	June 23	250°	50
3	32	12:44 (L+5)	June 23	14:00 (H.W.)	June 23	260°	90
2	32	13:00 (L+5)	June 23	14:53 (H+1)	June 23	260°	90
2	32	17:43 (H+4)	June 23	22:28 (L+3)	June 23	70°	40
3	32	19:44 (L.W.)	June 23	21:59 (L+2)	June 23	85°	25
1	15	21:49 (L+2)	June 23	0:09 (L+4)	June 24	275°	40
2	32	22:48 (L+3)	June 23	1:18 (L+5)	June 24	260°	25→95
1	21	6:02 (H+3)	July 24	7:52 (H+5)	July 24	70°	50
3	23	6:10 (H+3)	July 24	7:46 (H+5)	July 24	70°	60
2	26	22:51 (L+2)	July 24	0:46 (L+4)	July 25	90°	20
2	26	1:14 (L+4)	July 25	2:26 (L+5)	July 25	245°	60

Table 4.1

Table 4.1

Table 4.2

Station 75-4

CM	Depth (m)	From (EST)		To (EST)		Direction	Current (cm/sec)
3	24	12:39 (L+4)	June 24	13:29 (L+5)	June 24	240°	105
3	24	20:04 (H+5)	June 24	22:00 (L+2)	June 24	60°	105
1	14	1:19 (L+5)	June 25	3:37 (H+1)	June 25	230°	120
1	20	20:48 (L+1)	July 22	23:04 (L+4)	July 22	65°	90
3	24	23:26 (L+4)	July 22	2:36 (H+1)	July 23	230°	110

Table 4.2

Station 75-6

CM	Depth (m)	From (EST)		To (EST)		Direction	Current (cm/sec)
3	31	11:00 (L+4)	June 22	16:00 (H+3)	June 22	240°	110
2	33	11:00 (L+4)	June 22	16:00 (H+3)	June 22	240°	125
2	33	0:00 (L+5)	June 23	4:00 (H+2)	June 23	250°	180
1	16	3:00 (H+2)	June 23	6:00 (H+4)	June 23	$180^{\circ} \leftrightarrow 230^{\circ}$	$150 \longrightarrow 0$
2	25	11:43 (L+3)	July 23	16:23 (H+2)	July 23	245°	120
3	23	13:23 (L+5)	July 23	16:33 (H+2)	July 23	245°	100
3	23	17:28 (H+3)	July 23	20:33 (L.W.)	July 23	40°	95
1	20	19:22 (H+5)	July 23	21:22 (L+1)	July 23		
2	25	1:03 (L+5)	July 24	4:20 (H+2)	July 24	240°	140

Table 4.3

Table 4.3

Figure 4.2 groups all this information on one graph. Each event is represented at its recording depth by an arrow, the length of which shows the time interval of the oscillation. The direction of the arrow shows the current direction (flood or ebb) during this interval (flat lines are used when the tide is turning). When several arrows are superimposed the hatching inside the arrows is meant to differentiate their individual length.

From all of the above, five series were chosen to be studied in more detail. In Figure 4.3, we see the variability of the density field taken at two different depths (15 m and 32 m) for station 75-2. In considering the time series shown in Figure 4.3, it is perhaps time to make a distinction between what we have called "waves" and "oscillations". Internal waves (see Figure 4.3 from 12h50 to 13h10) are more organized than the oscillations preceding and following them. They have a larger amplitude and a well-defined periodicity (2-5 min). On the other hand, oscillations are characterized by an absence of structure and are of small amplitude. The less well-defined longer period oscillations (>5 min) will not be discussed, as this work is mainly concerned with higher frequency phenomena.

In most cases, oscillations of the density field start 2 to 3 hours before the current reaches its maximum speed and stop 2 to 3

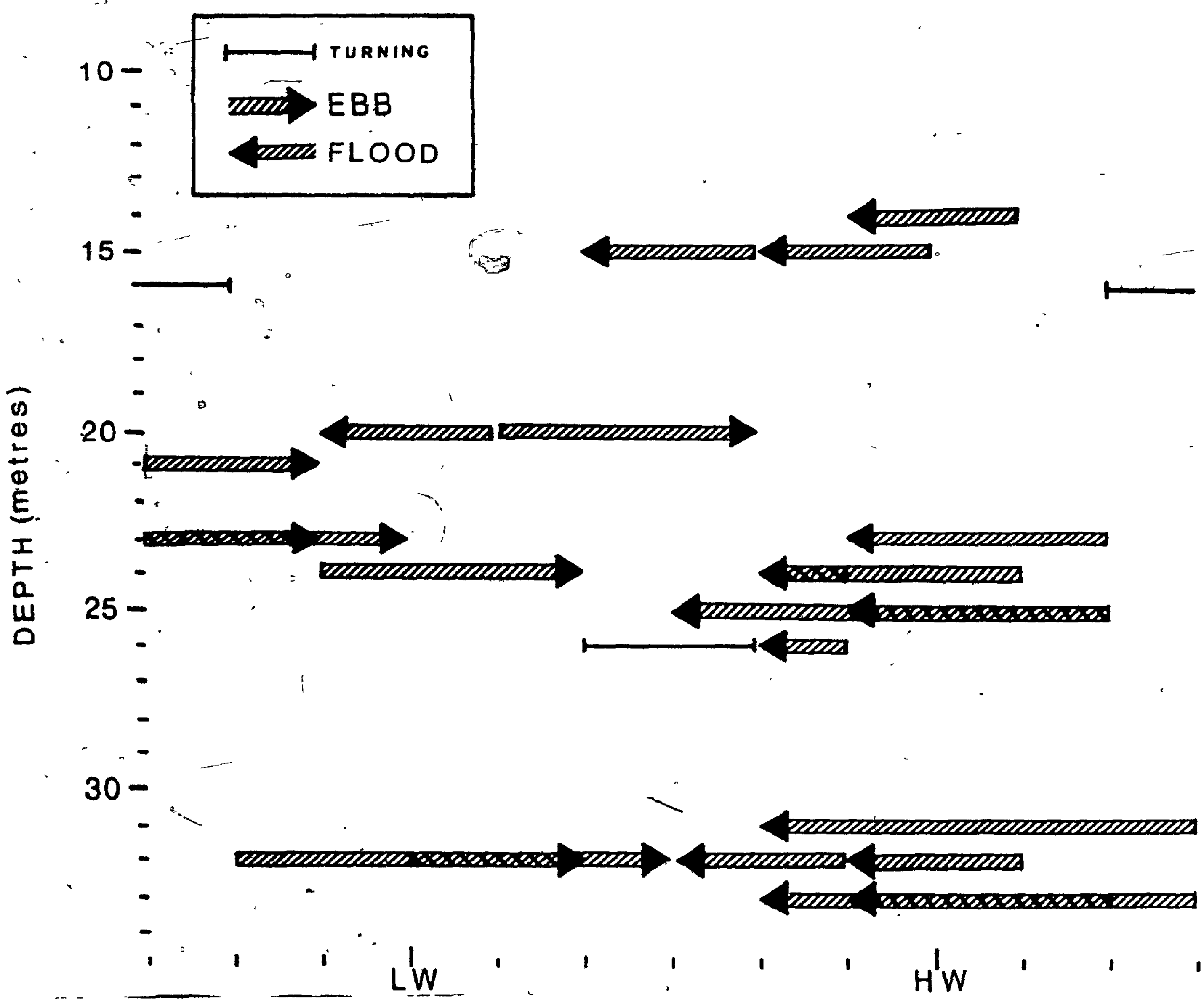

FIGURE 4.2 OBSERVED OSCILLATIONS

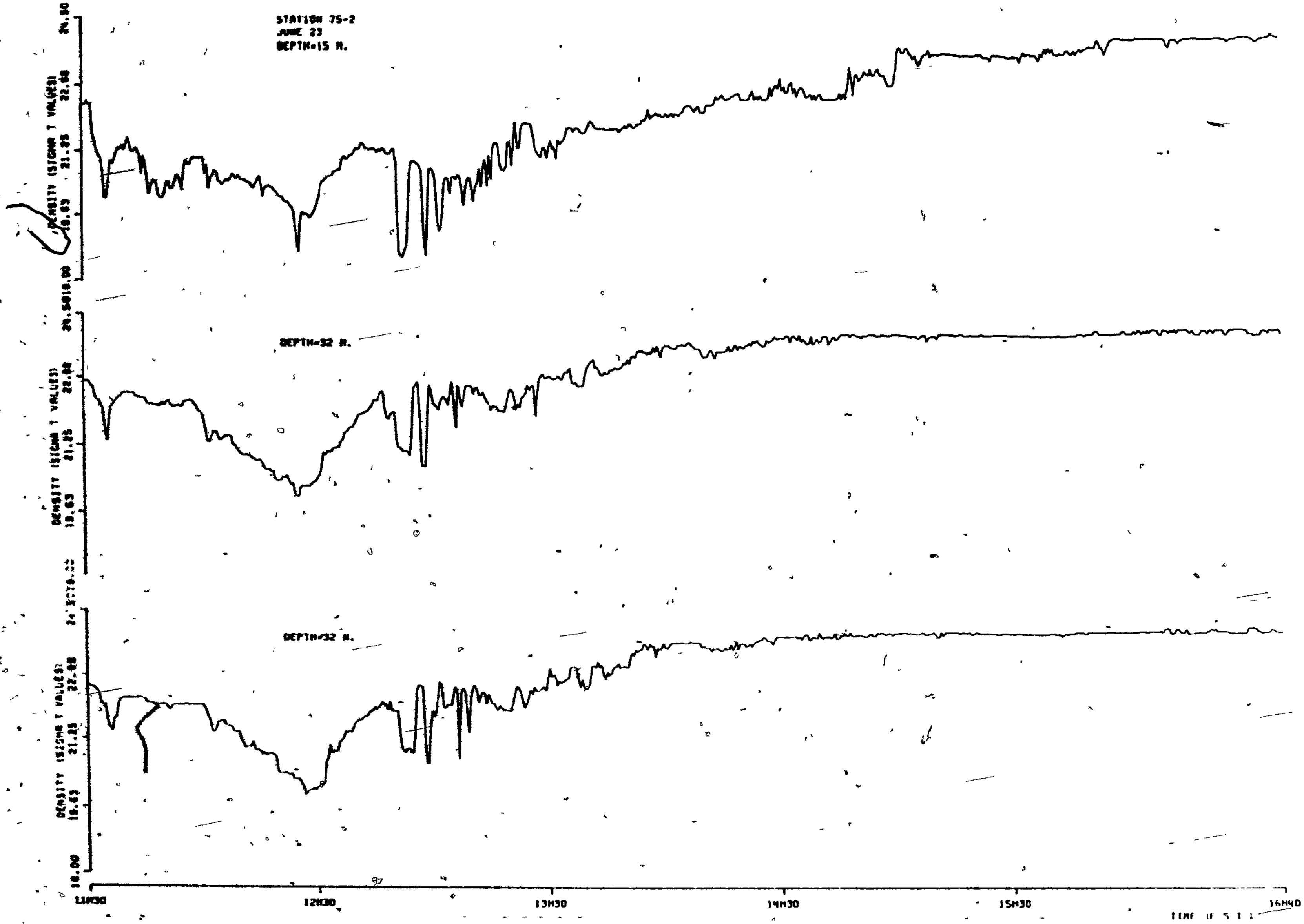

FIGURE 4.3 DENSITY VARIATIONS AT 75-2

hours after this maximum. Waves, in contrast to oscillations, are "short-lived", lasting from 10 to 20 minutes, and occur when the current has its largest value in the tidal cycle, corresponding to low values of J, the overall Richardson number (see Chapter 2 for a definition). It is also evident from Figure 4.2 that waves are created more often at flood than during ebb. This may be explained by the fact that the current is generally stronger during flood at our observation depths (see Figures 3.4, 3.5, 3.6). This corresponds to smaller values of J and more suitable conditions for the generation of waves. It was shown in Chapter 3, section 4, that the water on the upstream side of the bank was less stratified than on its downstream side, which may explain why internal waves are more frequent when the tide is flooding than when it is ebbing.

Returning our attention to Figure 4.3, we see that the same wave is recorded by three instruments at different locations: the top curve was taken at 15 m by CM 1, the centre curve at 32 m by CM 2, and the bottom one by CM 3 also at 32 m, but a certain distance behind the ship. Although the three curves are similar, the close resemblance between the centre and bottom curves is of special interest. A careful comparison of the two series between 12h50 and 13h10 shows an average lag of about 40 seconds. On considering the magnitude of the time lag, the imprecision in estimating the horizontal separation of the two instruments (see sect.4.1) and the 30 second sampling time of the current meters, it proved impossible to determine the wavelength. Furthermore, with all these limitations, one can only give the order of magnitude estimate of the phase speed of these waves as ~ 1 m/s.

Figure 4.4 shows the density and the Brunt-Väisälä frequency (N) profiles, as obtained from our STD record at 12h48, just before the arrival of the wave packet shown in Figure 4.3. There is only one maximum in the BV curve, at around 12 m. Table 4.4 lists the main features of the wave series, as measured by the top current meter (15 m depth) and the calculated range of $J = \frac{N^2 D^2}{U^2}$, which depends on

---

Station 75-2

15 m

June 23, 12h51 to 13h07

Frequency = 4.76×10^{-3} sec^{-1}

Period = 3.5 min

N (15 m) (12h48) = 5.45×10^{-2} sec^{-1}

$\overline{U}$ (15 m) = 36 cm/sec $\qquad$ $\overline{\theta}$ (15 m) = 257°

$12.87 < J < 27.25$

Table 4.4

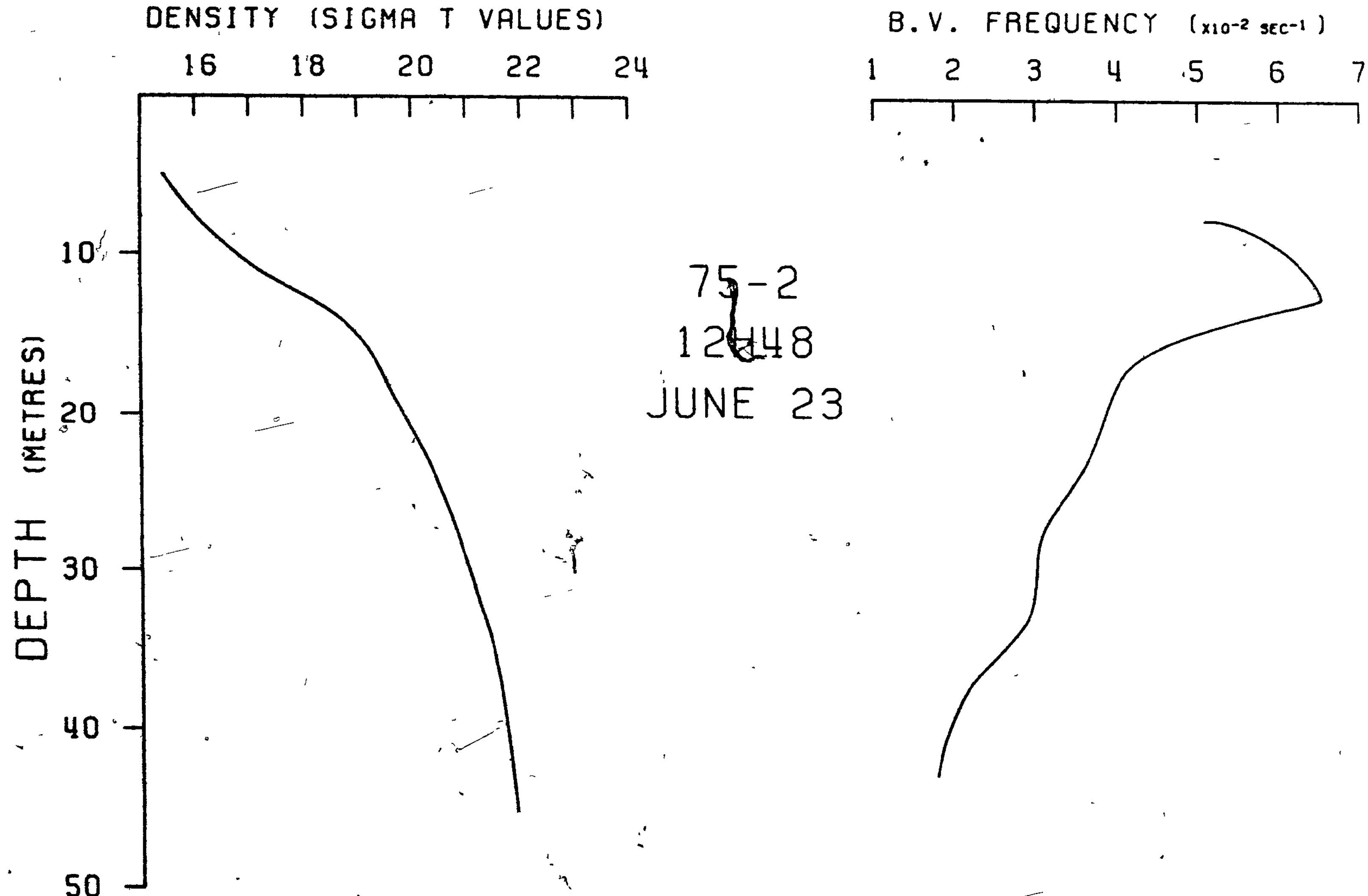

FIGURE 4.4 DENSITY AND B.V. FREQUENCY

the value taken for the total depth of the channel (85 m < D < 180 m). The value of J was calculated using the value of N at 15 m and the vector average speed ($\overline{U}$, $\overline{\theta}$) measured by the current meter during the interval the wave existed.

Although the frequency of the wave increases continuously, an estimate of its magnitude can be obtained by measuring the number of peaks observed over a short interval of time. This frequency and its related period are shown in Table 4.4. Note finally that $\overline{\theta}$, the average direction of the current, is in the "wrong" direction for these waves to be considered as a lee phenomenon at this station.

The series in Figure 4.5 were recorded at the same station and at the same depth (32 m) but 6 hours later, at the ebb. At this phase of the tide we find much larger variability in the density field than during flood. Attention will be focussed on the large amplitude waves occurring after 2018 EST. Here again, the lag in time between the two instruments is too small to permit any significant calculation of the wave length. The top curve is from CM 2 on line 1 attached to the ship and the bottom one is from CM 3 under the float. The only available density profile at this time was taken after the disappearance of the waves at 22h17 and is shown in Figure 4.6. It should be mentioned that no instantaneous picture of the oscillations was available on the ship from the current meters, as they were of the self-recording type

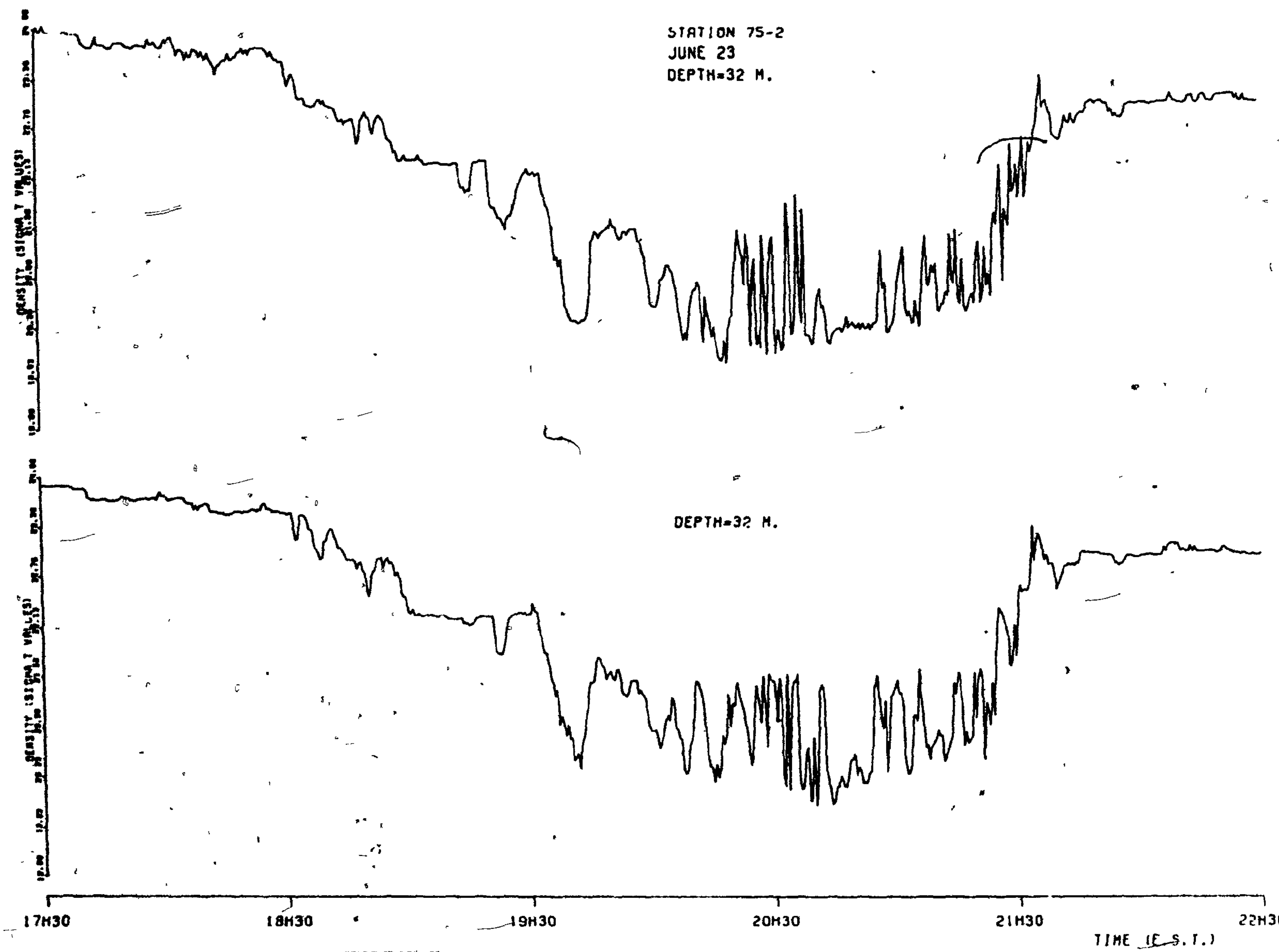

FIGURE 4.5 DENSITY VARIATIONS AT 75-2

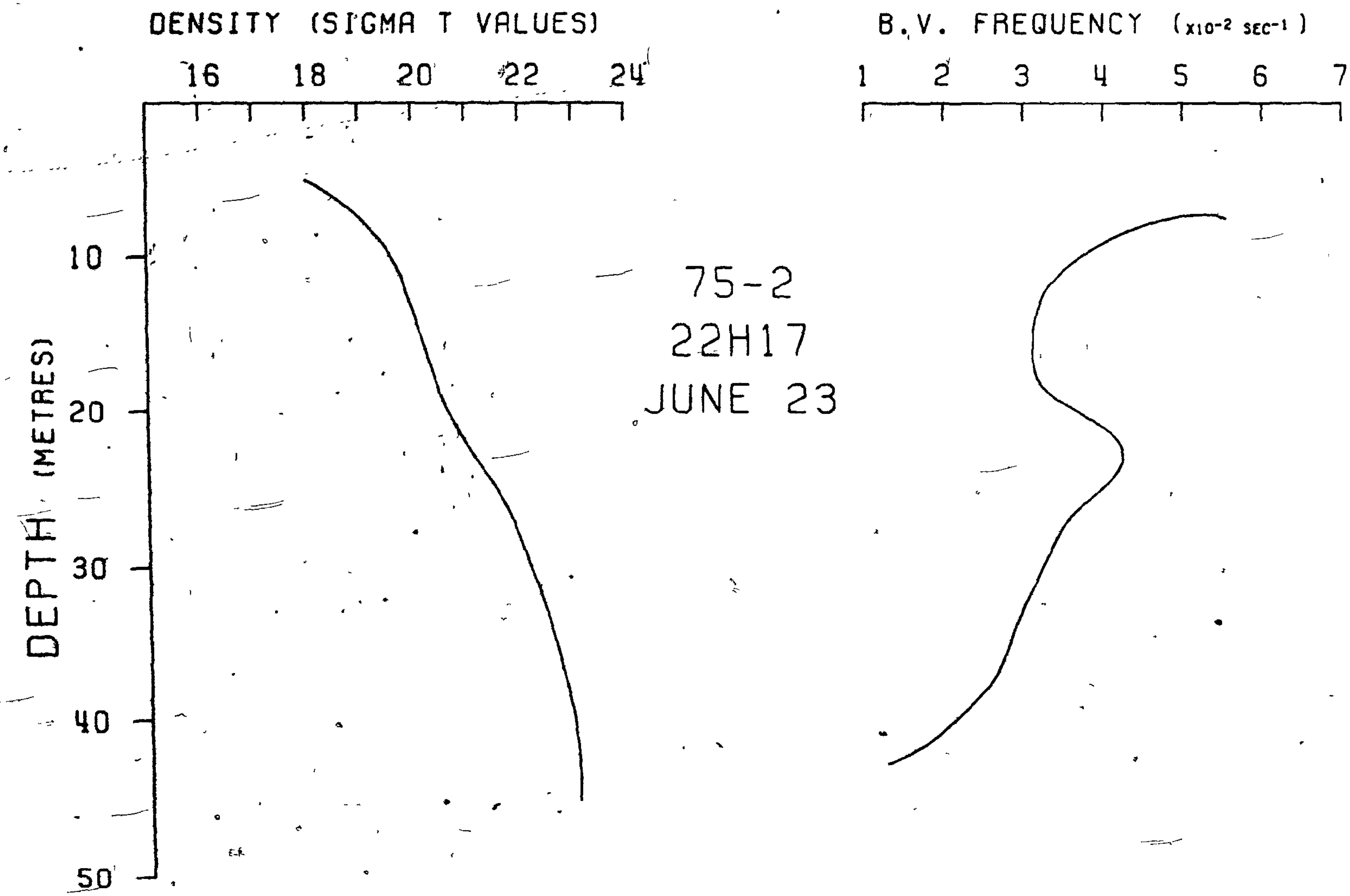

FIGURE 4.6 DENSITY AND B.V. FREQUENCY

Station 75-2

32 m

June 23, 20h18 to 20h38

Frequency = 6.73×10^{-3} sec^{-1}

Period = 2.48 min

N (32 m) (22h17) = 2.97×10^{-2} sec^{-1}

$\overline{U}$ (32 m) = 33 cm/sec $\overline{\theta}$ (32 m) = 88^0

$7.65 < J < 16.20$

Table 4.5

type and analysis of the magnetic tapes was done at a later date. In this instance, there is just one maximum of the BV frequency, at 23 m. However, the direction of the current (88^0) was appropriate for the generation of lee-waves. Wave frequency and other characteristics are given in Table 4.5.

In Figure 4.7, we see another example, this time taken at station 75-6. The top curve was from CM 3 at 23 m and the bottom one from CM 2 at 25 m. Thus, the current meters were at slightly different depths

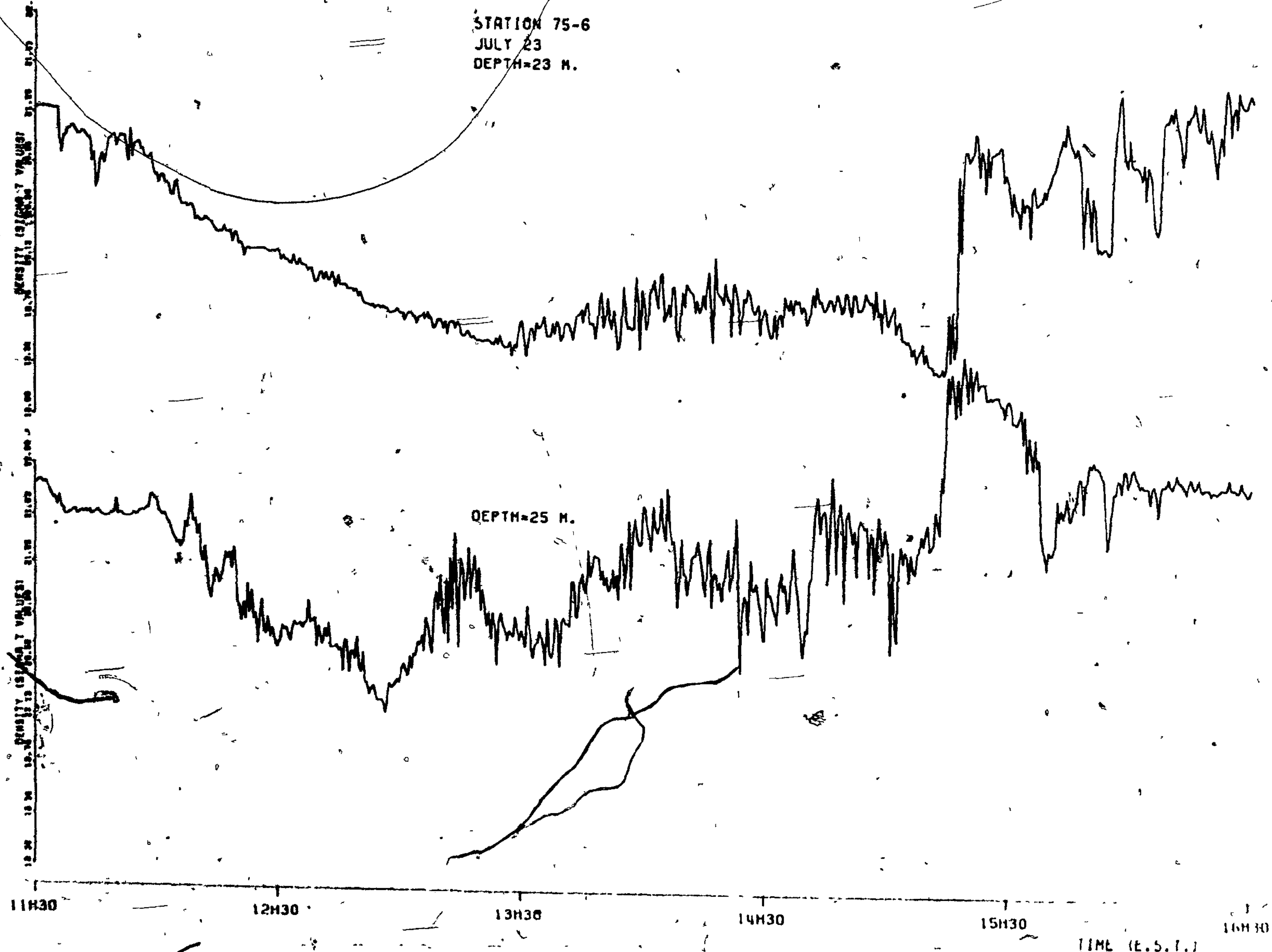

FIGURE 4-7 DENSITY VARIATIONS AT 75-6

and horizontally separated. The profiles in Figure 4.8 were taken when the waves were well established (14h08). Note the maximum of the BV frequency at 25 m and the minimum at 23 m and also how the amplitude of the wave at this depth (23 m) is smaller than the amplitude of the same wave two meters below. Judging from the variability we might expect to see similar changes in the shape of the curves plotted in Figure 4.8. As previously remarked in Chapter 3 (sect. 4), profiles are more complicated at this station than at 75-2. The wave properties at 25 m are given in Table 4.6. The high velocity and the low value of J should be noted. Although we have chosen to examine the waves occurring between 1354 and 1406 EST, one can see a sizeable amount of high frequency variability in the 45 minutes preceding the

---

Station 75-6

25 m

July 23, 13h54 to 14h06

Frequency = 8.70×10^{-3} sec^{-1}

Period = 1.92 min

N (25 m) = 4.80×10^{-2} sec^{-1}
(14h08)

$\overline{U}$ (25 m) = 144 cm/sec $\overline{\theta}$ (25 m) = 247°

$2.83 < J < 6.00$

Table 4.6

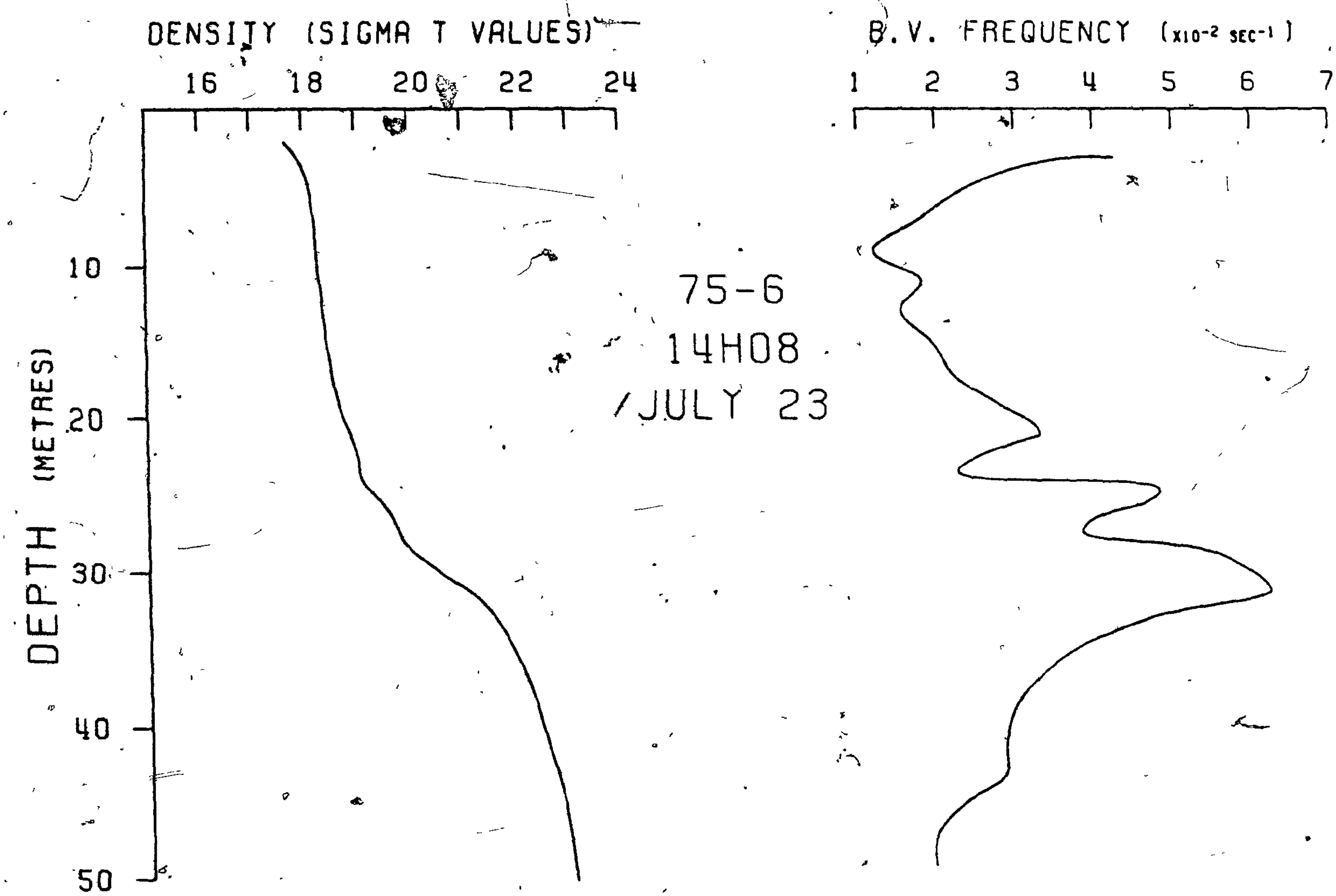

FIGURE 4.8 DENSITY AND B.V. FREQUENCY

passage of a front-like phenomenon at 1515 in Figure 4.7.

Figure 4.9 shows us one of the most striking sets of observations obtained from our measurements. The presence of such waves at station 75-4 would indicate that the top of the obstacle is possibly the best place to observe large-amplitude waves. In Figure 4.10, the characteristics of the water column immediately after the waves disappeared are shown. Wave properties are given in Table 4.7. As before, a large current and a low value of J was found. Because of the shallow depth at station 75-4, one might expect to observe the highest current velocities (compare Figures 3.4, 3.5, 3.6).

Station 75-4

24 m

July 23, 1h04.7 to 1h23.7

Frequency = 7.89×10^{-3} sec^{-1}

Period = 2.11 min

N (24 m) (1h37) = 3.46×10^{-2} sec^{-1}

$\overline{U}$ (24 m) = 117 cm/sec $\overline{\theta}$ (24 m) = 240°

$2.51 < J < 5.32$

Table 4.7

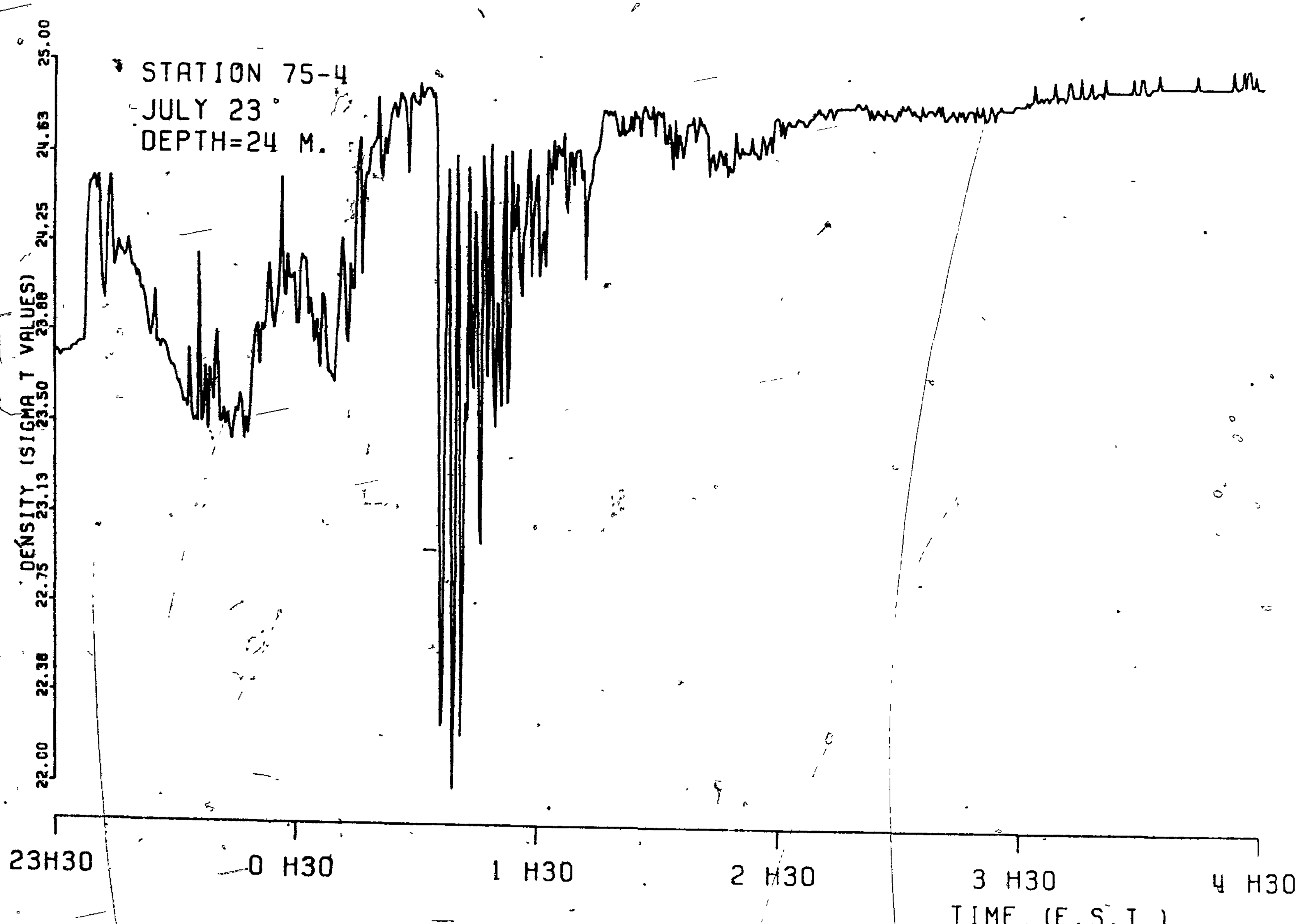

FIGURE 4.9 DENSITY VARIATIONS AT 75-4

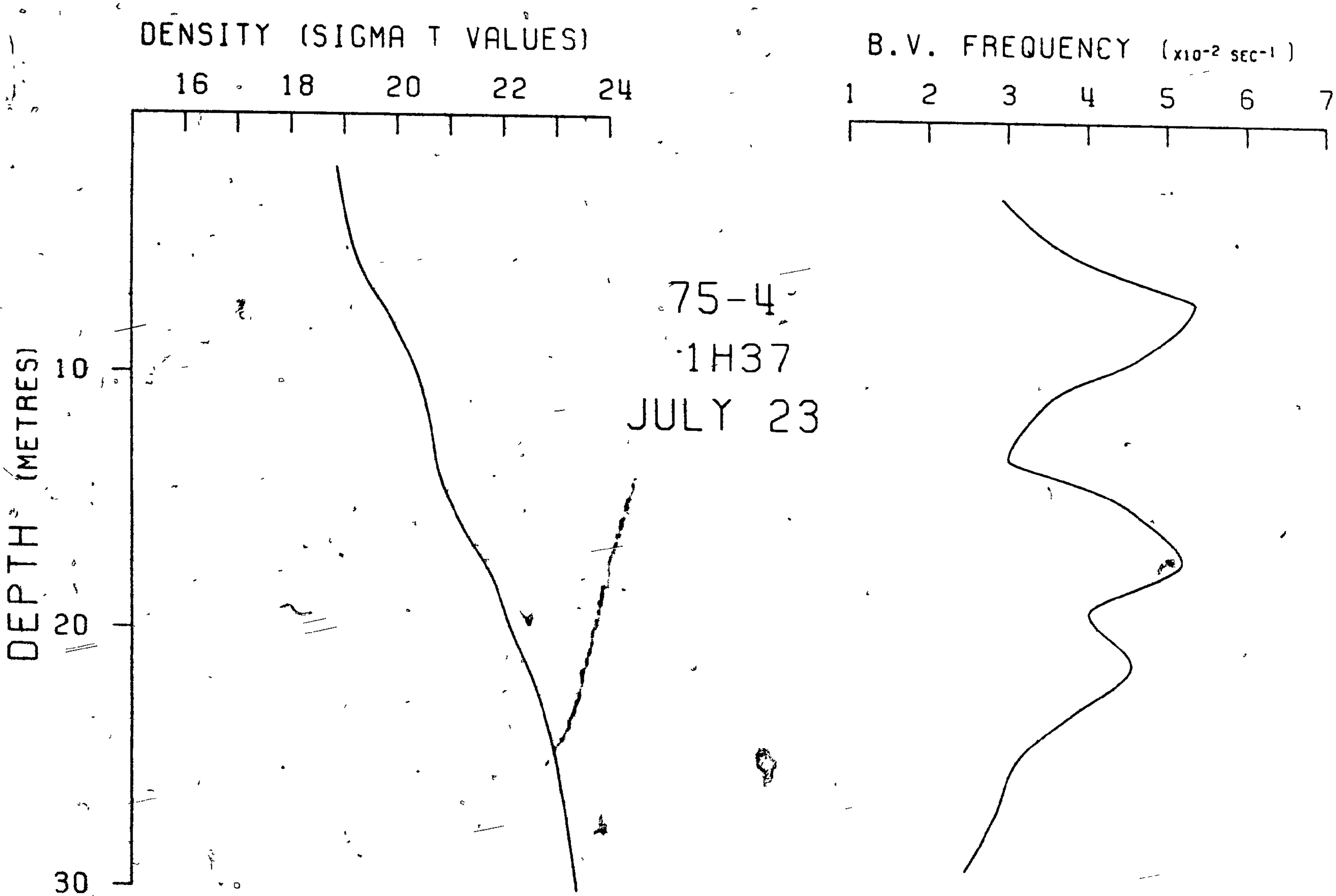

FIGURE 4.10 DENSITY AND B.V. FREQUENCY

In our last example, Figure 4.11 shows another case of internal waves measured at two different depths and separated horizontally from one another. The top curve was recorded by CM 2 under the ship and the bottom curve by CM 3 a certain distance away. Figure 4.12 and Table 4.8 give the related profiles and properties.

Station 75-2

23 m

July 24, 6h53 to 7h08

Frequency = 6.45×10^{-3} sec^{-1}

Period = 2.58 min

N (23 m) (6h56) = 3.25×10^{-2} sec^{-1}

$\overline{U}$ (23 m) = 75 cm/sec $\qquad$ $\overline{\theta}$ (23 m) = 64^{o}

$3.68 < J < 7.80$

Table 4.8

Note the absence of waves (from 6h53 to 7h08) at the lower depth, just three meters below. From this record, one has either an indication

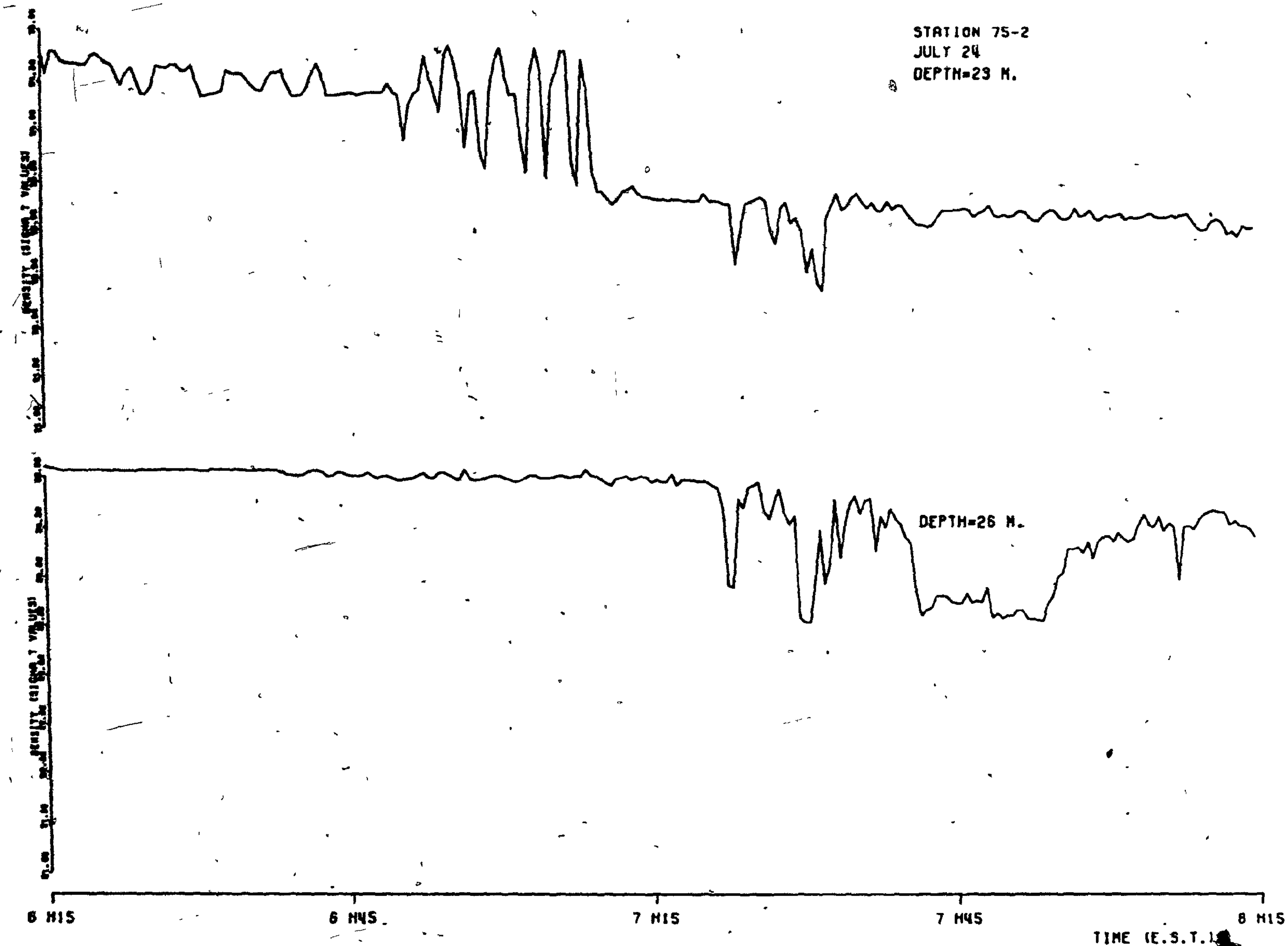

FIGURE 4.11 DENSITY VARIATIONS AT 75-2

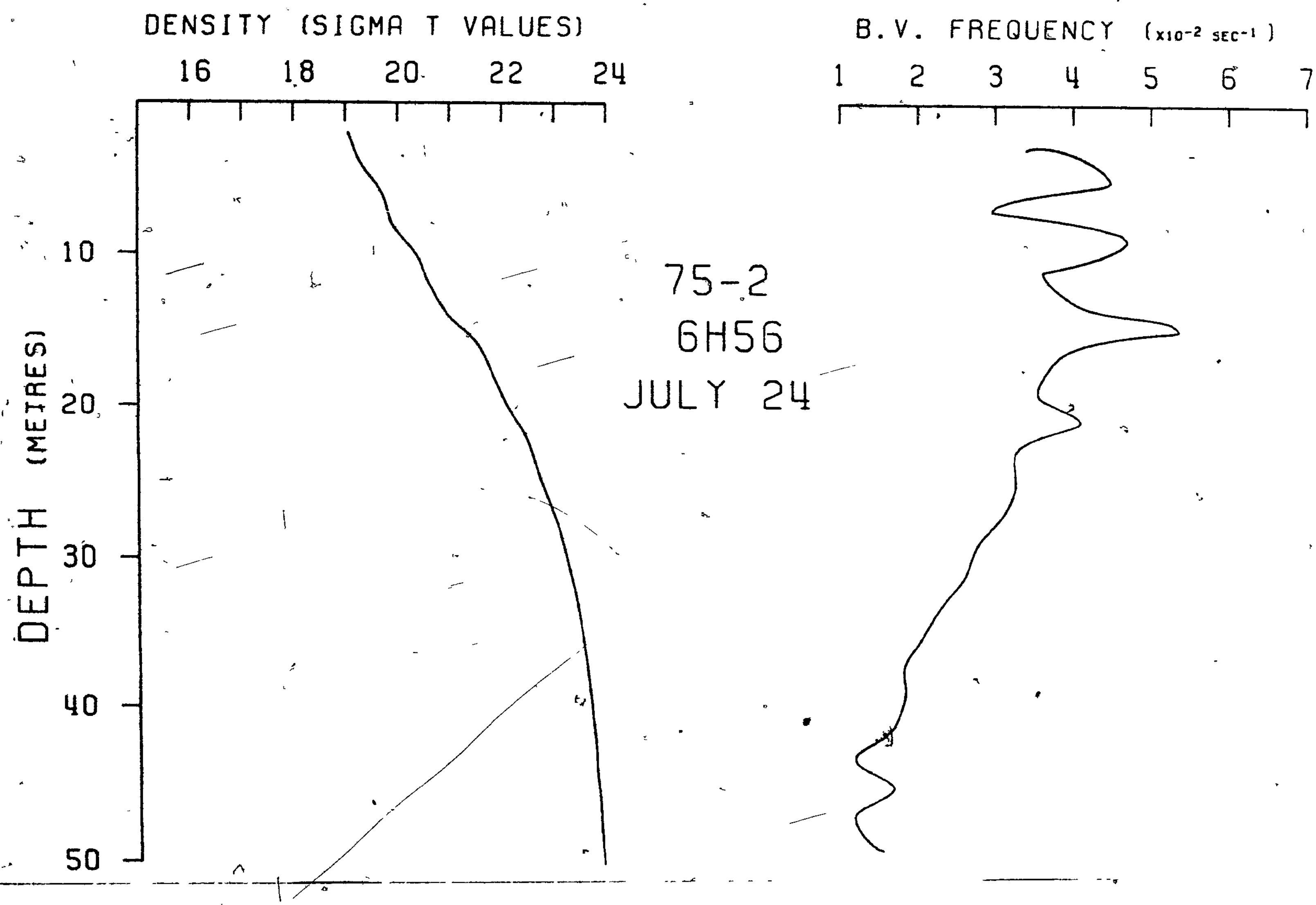

FIGURE 4.12 DENSITY AND B.V. FREQUENCY

of the wave amplitude or the possibility of a dampening mechanism which prevents the wave energy from propagating to lower levels.

4.3 DISCUSSION

Although one of the original aims of this research program was to describe the characteristics of internal waves in the lee of an obstacle, we were unable to successfully complete this aspect of the study. The individual wave series have been well described as a function of time, but poorly in space. Aanderaa current meters, with a 30 second sampling time, were deployed in a triangular array (x - z plane) to determine both spatial and temporal characteristics. As a result of geometric changes in the array and the relatively slow sampling rate, the phase velocity or wavelength could not be estimated with any confidence. The observations do imply that "classical" lee waves were not present. However, the results suggest that the internal waves recorded in this area of the St. Lawrence estuary may result from the presence of the sill, either through changes of local velocity shear, blocking, non-linear effects, or stratification changes, etc. For example, waves were observed in front of the obstacle during flood at station 75-2 and during ebb at 75-6 (see underlined values in Tables 4.1 to 4.3 for all such cases), suggesting some other mechanism than lee-waves (similar to Long's work) for their generation. It is known, experimentally and theoretically, that the influence of a barrier on the flow will allow waves to propagate on both the lee side and upstream ("blocking"). Trustrum (1964) described the "blocking" in this way: "the upstream solutions are periodic in z and independent of x, and therefore describe one-dimensional flows extending to $x = +\infty$ (the columnar modes)". Turner (1973), presenting the same phenomenon, explains in his book that "... what is observed experimentally just after such a body (the barrier in the lab model) is set into slow motion is not so simple, however. In addition to a plug of finite length directly ahead of the body, an array of alternating jets develops at other horizontal levels. These jets become more numerous as $F = 1/J$ is reduced, and they all propagate upstream in time, altering the approaching flow."

These two descriptions of the "blocking" ahead of the obstacle were made for a steady state. If the flow (F) is allowed to vary in time (as it does in our case) the number and the height of these jets will vary in time, providing to an observer at a fixed depth the kind of oscillations obtained in our series (vertical motion of the water particles) ahead of the obstacle. Another possibility to explain these "upstream waves" comes from Long's laboratory experiments. In several of his pictures and graphs of the flow it can be seen that at the top of (as at 75-4) or close to the edge of the obstacle (as at 75-2 and 75-6) one will be ahead of the 'plug' described by Turner and in the wave itself. The wave is created by the entire obstacle, not just by one of its sides. Unfortunately, stations 75-2 and 75-6 were too close to the barrier to properly discriminate between lee-waves and upstream blocking. If this is true, it is not surprising to observe oscillations when the conditions (current direction and J) are inappropriate: they are just the deformed prolongation of a wave created on the opposite side of the sill. Our vessel could not be anchored in the deeper region of the basin downstream of Pointe-au-Pic, where the most suitable observations may have been made.

Although it was not possible to determine the direction of wave propagation in most cases, the records are suggestive of propagating internal waves, probably large amplitude, similar to those described by Halpern (1971) and Gargett (1976). Both of these authors found a series of internal waves associated with the arrival of a warm front in the upper layers. The waves were characterized by long flat crests and sharp narrow troughs. Both Gargett and Lee and Beardsley's (1974) analysis of Halpern's data suggest that the generated waves are of the solitary type. They were generated at the frontal boundary by non-linear steepening of the interface and subsequent effects of dispersion and non-linearity.

For the examples shown herein, there is only one instance of an internal wave train accompanying a deepening of the isopycnals. Every other case shows an appearance of waves at the time of a rise in the mean density. This relationship is most clearly seen in Figure 3.18, where large amplitude oscillations of the density field are observed at the time of sharp increases in the mean density. At this site, the occurrence of waves was dependent on the time rate of density change. Wave generation was found only during front-like increases of density. No oscillations are seen when the density values increase gradually. Because of the alternating pattern found in the temporal variation of density, waves were generated during the flood at station 75-11 with a diurnal periodicity. At the other stations, appearance of waves was not so easily related to changes in the mean conditions. The possibility of rapid density changes at all sites during both ebb and flood can be seen by examining the isopycnal distribution in Figure 3.17. In Figures 4.3, 4.5, 4.7 and 4.9 a high degree of variability is found immediately before increases of density were recorded. For most of the cases mentioned, the density shift is abrupt, resembling a front. Thus, it can be seen that in the present work conditions differ from those reported by Halpern and Gargett. Instead of a surface front preceding less dense water, there exists a sub-surface front of denser water in the lower half of the column. Theoretically, the analysis by Lee and Beardsley (1974) must be altered to include the case for a deep front of higher density. Under appropriate conditions, a train of solitary waves, exhibiting sharp crests and flat troughs, may be generated in this depth interval. Waves with these characteristics can be seen in Figures 4.5 and 4.7. Also seen in these and the other figures are both symmetric waves and waves with flat crests and sharp troughs. Depending on the non-linear and dispersive effects, solitary or non-solitary internal waves may be generated. At mid-depth locations, symmetric waves are quite likely. The presence of solitary waves does offer an explanation for the decreasing time between crests, as crest speed is a function of wave height and the individual peaks arrive non-periodically (see Lee and Beardsley, 1974). Since the amplitude of the fronts and the waves is not known, as well as the wavelength, it is not possible to directly compare the theoretical predictions and the field observations.

Thus, it was difficult to separate waves generated by "upstream influence", steepening of an internal density front or "lee wave" processes. In many of the observations, the generation of internal waves, either solitary or non-solitary, at an internal density front seemed to provide a plausible explanation. At other times, the density characteristics were suggestive of different mechanisms, possibly those mentioned above.

In summary, numerous points can be made concerning the waves found in the region of our study:

(i) The internal waves (not the oscillations seen before and after) exist for a short time, typically 15 minutes;

(ii) They are of a short period (or high frequency), varying between 2 and 4 minutes;

(iii) Longer period internal oscillations of tidal (semi-diurnal and diurnal) origin are also present in the density field, but have not been treated in the present work;

(iv) Contrary to the prediction of lee-wave theory (in Chapter 2), the frequency of the observed waves was found to increase continuously. The calculated frequency was always smaller than the local N (Brunt-Väisälä);

(v) The vertical distribution of the waves presented gives us a further insight into their properties. As suggested by many theories, these waves seem to be generated where the BV frequency is a maximum. In fact, observations of the density above the BV frequency maximum level show the appearance of denser water pushed by the wave into the higher level (e.g. Figure 4.5). Observations below the maximum BV level show an incursion of less dense water at this level (e.g. Figure 4.9). Finally, at the generation level a symmetrical pattern (upward and downward) is observed (e.g. Figure 4.11);

(vi) As predicted by Long, values of J (the overall Richardson number) are usually low, mainly because waves always occur when the currents are strong;

(vii) There is strong evidence of upstream propagation of the waves at least 10 km from their suspected source (the obstacle in the channel);

(viii) The waves characteristics often resemble those found by others in shallow areas, and have the form of a series of "solitary-like" waves, whose propagation speed is dependent on wave amplitude. On these occasions, the waves preceded the arrival of a front-like change of density. At the depth of the present observations, density increases over the front were more common.

CHAPTER 5

CONCLUSION

In this chapter, the general characteristics of the region will be summarized and the main properties of the internal waves found there will be presented. A few suggestions for further investigation follow this discussion.

The region is characterized by strong tidal currents during flood, with a maximum sub-surface velocity of 180 cm/sec over the sill. The main bathymetric feature is the English Bank, an extension of which obstructs the channel running along the north shore of the river, near Pointe-au-Pic. The Bank divides the circulation into two main flows, one passing to the south and the other to the north. The flood ends 3 to 4 hours after high tide at Pointe-au-Père, while the low water slack occurs 2 to 3 hours after low tide. The vertical shear of the horizontal velocity rarely exceeded 0.1 sec^{-1}, as measured in the summer of 1974 by the CCIW (the average never exceeds 0.01 sec^{-1}).

Vertical stratification of the water column is relatively weak in this part of the estuary. Density values near Pointe-au-Pic change almost linearly with depth below 20 m, except during flood in the area upstream of English Bank. Values are characteristic of those found in an estuary, with σ_t varying between 13 and 25.

For almost every semi-diurnal tide, when the current is near its maximum velocity, internal waves are formed in the narrow passage between the English Bank and the mainland. These waves exist for 10 to 20 minutes and have a period of 2 to 4 minutes. At the mooring site, waves were generated with diurnal periodicity, this resulting from the differing density characteristics between successive semi-diurnal tides.

In light of the different theories presented, most of the density fluctuations shown in Chapter 4 seem to be related to the influence of the local bottom topography (English Bank). Furthermore, as these waves closely resemble those described by Halpern (1971), the most acceptable explanation for their generation is the instability of the flow as it passes over English Bank from either direction. In all of the present examples, waves were accompanied by an abrupt change in density. Lee and Beardsley (1974) suggest that density fronts like these become non-linear and form waves due to the interplay of dispersion and non-linearity. Unlike their work, waves were observed during an intrusion of both more dense and less dense water masses. Depending on the local depth and stratification, internal waves of the solitary or non-solitary type could be formed.

As Long (1955) had predicted, internal waves were observed in the lee of the barrier only when the overall Richardson number, J, was smaller than π (see Figures 4.7, 4.9, 4.11). As our measurements were limited in number, and because of the height of the obstacle relative to downstream depth to the flow, Bell's (1975) predictions cannot be tested using the present observations.

As discussed in Chapter 2, the waves created in such a dispersive medium as the estuary and by such a large obstacle become rapidly non-linear. The asymmetric shape of the waves given as examples in Chapter 4 are effectively non-linear: density values at a given depth always start from some basic level and rapidly reach a higher or lower level (example: Figure 4.9). The relative sign of this peak (positive or negative) depends on the distribution of the BV frequency N and other factors. If N_{max} is above the observation level, incursion of less dense water is recorded by the instrument and negative peaks result; if the N_{max} level is deeper than the instrument, denser water goes up to the current meter and positive peaks are recorded. Thus it is inferred that internal waves are produced at a level of maximum N.

Some of the internal waves observed were probably of the solitary type, as described by Halpern (1971), Lee and Beardsley (1974) and Gargett (1976). If this classification is justified, the speed of each crest (an independent wave) is proportional to its amplitude. As the waves following the leading wave are of smaller amplitude, they travel at smaller speeds. Unfortunately, no reliable measure of wave amplitude was obtained, but the speed variation (and thus separation) between each wave can be used to explain the frequency increase found in the present work. According to prediction, this distance (as measured at one location) diminishes between the succeeding waves of lower amplitude. Without a reliable estimate of wavelength, Doppler shifting of the observed frequency by the mean flow could not be determined.

Although the direction of wave propagation is unknown, it is evident that internal waves created over the English Bank propagate in both directions, upstream and downstream, for at least 5-10 km away from the top of the obstacle. As an example, the oscillations shown in Figure 4.3 did not occur in the lee of the obstacle (relative to the current direction at this time) but ahead of it. In general, it was difficult to separate waves generated at a steepening internal front from upstream influences or advected lee waves because of a lack of supporting data. The results do indicate that internal fronts are the most likely source. No definite conclusions can be drawn from the observations about the presence of a "columnar mode".

In regard to the above conclusions, it should be remembered that velocity shears were not measured uniformly over the water column and that S.T.D. profiles were not taken simultaneously with the arrival of the internal waves. Therefore, the stability and water stratification (and thus the BV frequency distribution) are not always known at the time that waves were recorded. Simultaneity of all observations would have allowed for a more rigorous analysis and perhaps more interesting conclusions.

A few suggestions for the preparation of a more complete experimental program to study the formation and behaviour of these waves will now be given. Simultaneous observations on both sides of the obstacle (the English Bank) should be undertaken, but sufficiently far away so as to discriminate clearly between stationary lee waves, propagating internal (small-amplitude) wave groups, and solitary wave trains, from their upstream disturbances. Density and current profiles should be taken regularly at a 30 minute interval or less. Wavelength, crest speed and amplitude of the internal waves should be measured. As the speed of wave propagation is faster than we have anticipated, either the sampling rate should be increased or the separation distance of the sensors lengthened. The geometry of the sensor array must remain constant. This could be done by mooring closely spaced current meter strings. Data obtained in this manner would be used to supplement the shipboard observations. "Real time" observation of the waves would allow for increased sampling during intervals of particular interest.

BIBLIOGRAPHY

BELL, T.H., 1975: Lee waves in stratified flows with single harmonic time dependence. J. Fluid Mech. 67, p. 705.

BENJAMIN, T.B., 1966: Internal waves of finite amplitude and permanent form. J. Fluid Mech. 25, p. 241.

BENNEY, D.J., 1966: Long nonlinear waves in fluid flows. J. Math. Phys. 45, p. 52.

BUDGELL, W.P. and MUIR, L.R., 1975: St. Lawrence River Current Survey 1974. Data report, Unpublished manuscript of the Canada Centre for Inland Waters, Burlington, Ontario.

CANADIAN HYDROGRAPHIC SERVICE, 1939: Tidal Current Charts - St. Lawrence Estuary - Orleans I. to Father Point. CHS, Survey and Mapping Branch, Department of Mines and Technical Surveys, Ottawa.

____________________, 1975: Canadian Tide and Current Tables, Volume 3, St. Lawrence and Saguenay Rivers. CHS, Marine Sciences Directorate, Department of the Environment, Ottawa.

ERDELYI, A., 1956: Asymptotic Expansions. New York: Dover.

FORRESTER, W.D., 1974: Internal tides in St. Lawrence estuary. J. Mar. Res. 32, p. 55.

GARGETT, A.E., 1976: Generation of Internal Waves in the Strait of Georgia, British Columbia. Deep-Sea Res. 23, p. 22.

HALPERN, D., 1971: Observations on short period internal waves in Massachusetts Bay. J. Mar. Res. 29, p. 116.

HOWARD, L.N., 1961: Note on a paper of John W. Miles. J. Fluid Mech. 10, p. 509.

HUPPERT, H.E. and MILES, J.W., 1969: Lee Waves in a Stratified Flow, Part 3 - Semi-elliptical obstacle. J. Fluid Mech. 35, pp.481-6.

LEE, C.Y. and BEARDSLEY, R.C., 1974: The generation of long non-linear internal waves in a weakly stratified shear flow. J. Geo. Res. 79, p. 453.

LONG, R.R., 1953: Some Aspects of the Flow of Stratified Fluids. I - A Theoretical Investigation. Tellus 5, pp. 42-57.

________, 1955: Some Aspects of the Flow of Stratified Fluids. III - Continuous Density Gradient. Tellus 7, pp. 342-57.

________, 1970: Blocking effects in flow over obstacles. Tellus 12, p. 471.

MILES, J.W., 1963: On the Stability of Heterogeneous Shear Flows. Part 2, J. Fluid Mech. 16, pp. 209-27.

McINTYRE, M.E., 1972: On Long's Hypothesis of no upstream influence in uniformly stratified or rotating flow. J. Fluid Mech. 52, pp.209-43.

PHILLIPS, O.M., 1966: The Dynamics of the Upper Ocean. Cambridge University Press.

THORPE, S.A., 1975: The Excitation, Dissipation and Interaction of Internal Waves in the Deep Ocean. J. Geophys. Res. 80, pp. 328-38.

TRUSTRUM, K., 1964: Rotating and Stratified Fluid Flow. J. Fluid Mech. 19, pp. 415-32.

TURNER, J.S., 1973: Buoyancy Effects in Fluids. Cambridge University Press.

ZABUSKY, N.J. and KRUSKAL, M.D., 1965: Interaction of "solitons" in a collisionless plasma and the recurrence of initial states. Phys. Rev. Letters, 15, pp. 240-43.

APPENDIX 1: List of Stations

Station		Latitude (N)	Longitude (W)
75-2	○	47°39.1'	70°03.4'
75-4	○	47°37.5'	70°06.7'
75-6	○	47°35.0'	70°09.3'
75-11	■	47°38.7'	70°04.4'
74-12c-01	■	47°30'15"	70°12'01"
74-12c-04	■	47°27'54"	70°07'10"
74-12c-07	⊡	47°38'06"	69°57'05"
74-12c-11	■	47°45'36"	69°51'30"
10	△	47°40'54"	70°01'12"
11	△	47°40'30"	70°00'12"
31	△	47°38'30"	70°04'24"
36	△	47°36'42"	70°08'18"
37	△	47°35'54"	70°06'42"
43	△	47°38'48"	70°07'00"
STA 63	⬡	47°37'04"	70°07'44"

⊡ 2 months mooring
■ 1 month mooring
□ 3 days mooring
⬡ CHS tidal survey station (1934-37)
○ 13 to 22 hours fixed station
△ 13 hours profiling station

APPENDIX 2: Tidal Prediction at Pointe-au-Père

$(48^{o}31'N - 68^{o}28'W)$

	Hour (EST)	Height (M)		Hour (EST)	Height (M)
June 22	0:45	4.1	July 22	1:20	4.1
	9:20	0.7		7:55	0.7
	13:25	3.4		13:45	3.4
	19:00	1.0		19:35	1.0
June 23	1:30	4.3	July 23	2:00	4.2
	8:05	0.6		8:35	0.7
	14:10	3.5		14:25	3.5
	19:45	0.9		20:20	0.9
June 24	2:10	4.4	July 24	2:40	4.2
	8:45	0.5		9:15	0.6
	14:50	3.5		15:05	3.5
	20:35	0.9		20:50	0.9
June 25	4:50	4.4	July 25	3:05	4.2
	9:30	0.6		9:30	0.7